Deciphering evolutionary trajectories of lactate dehydrogenases provides new insights into allostery.

Adeline Robin, Céline Brochier-Armanet, Quentin Bertrand, Caroline Barette, Eric Girard, Dominique Madern

Deciphering evolutionary trajectories of lactate dehydrogenases provides new insights into allostery.

Adeline Y. Robin[1], Céline Brochier-Armanet[2]; Quentin Bertrand[1,3], Caroline Barette[4], Eric Girard[1]*, and Dominique Madern[1]*

1-Univ. Grenoble Alpes, CEA, CNRS, IBS, 38000 Grenoble, France

2-Université Claude Bernard Lyon 1, CNRS, UMR5558, Laboratoire de Biométrie et Biologie Évolutive, 43 bd du 11 novembre 1918, F-69622, Villeurbanne, France.

3-Laboratory of Biomolecular Research, Biology and Chemistry Division, Paul Scherrer Institut, Villigen, Switzerland.

4-Univ. Grenoble Alpes, CEA, Inserm, IRIG, BGE, 38000 Grenoble, France.

* Corresponding authors:

Drs Dominique Madern, and Eric Girard

Email: dominique.madern @ ibs.fr; eric.girard @ ibs.fr

Abstract

Lactate dehydrogenase (LDH, EC.1.1.127) is an important enzyme engaged in the anaerobic metabolism of cells, catalyzing the conversion of pyruvate to lactate and NADH to NAD^+.

LDH is a relevant enzyme to investigate structure-function relationships. The present work provides the missing link in our understanding of the evolution of LDHs. This allows to explain i) the various evolutionary origins of LDHs in eukaryotic cells and their further diversification, as well as ii) subtle phenotypic modifications with respect to their regulation capacity.

We identified a group of cyanobacterial LDHs displaying eukaryotic-like LDH sequence features. The biochemical and structural characterization of *Cyanobacterium aponinum* LDH, taken as representative, unexpectedly revealed that it displays homotropic and heterotropic activation, typical of an allosteric enzyme, whereas it harbors a long N-terminal extension, a structural feature considered responsible for the lack of allosteric capacity in eukaryotic LDHs. Its crystallographic structure was solved in two different configurations typical of the R-active and T-inactive states encountered in allosteric LDHs.

Structural comparisons coupled with our evolutionary analyses helped to identify two amino acid positions that could have had a major role in the attenuation and extinction of the allosteric activation in eukaryotic LDHs rather than the presence of the N-terminal extension.

We tested this hypothesis by site-directed mutagenesis. The resulting *Cyanobacterium aponinum* LDH mutants displayed reduced allosteric capacity mimicking those encountered in plants and human LDHs.

This study provides a new evolutionary scenario of LDHs that unifies descriptions of regulatory properties with structural and mutational patterns of these important enzymes.

Introduction

Lactate dehydrogenases are critical enzymes (LDHs, EC.1.1.127) involved in the anaerobic metabolism of cells. They are mainly present in eukaryotes and bacteria, while they are rare in archaea. LDHs from different species were purified and characterized (Brochier-Armanet and Madern 2021, and references therein). They operate in the last step of glycolysis by catalyzing the reversible chemical transformation of pyruvate into lactate with NADH as coenzyme (Everse and Kaplan 1973; Holbrook et al., 1975; Fersht, 1985). From a functional point of view, LDHs allow the regeneration of NAD^+ and thus sustain the glucose catabolism of cells under conditions of limited oxygen concentration (Everse and Kaplan 1973; Holbrook et al., 1975; Fersht 1985). The catalytic mechanism of LDHs has been extensively studied. When the competent catalytic state is reached, LDHs catalyze the direct transfer of a hydride ion from the pro-R face of NADH to the C2 carbon of pyruvate to produce lactate (Burgner and Ray, 1984; Clarke et al., 1986; Clarke et al. 1988; van Beek et al. 1997; Deng et al. 2011, Callender and Dyer, 2015; Egawa et al. 2019). This reaction is controlled by a rate-limiting step due to the closing of a mobile loop (MbL), which covers the catalytic vacuole (Clarke et al., 1985; Pineda et al. 2007). The MbL carries also a glutamine residue at position 102 (Q102) that plays a key role in substrate recognition and specificity (Wilks et al. 1982; Cendrin et al. 1993; Katava et al. 2020).

LDHs are homotetrameric enzymes with the four subunits related by three molecular 2-fold axes named P, Q, and R (Rossmann et al. 1973). Crystal structures show that tetrameric LDHs have four active sites. The active site of each subunit lies near the Q-axis interface and involves mainly H68, Q102, R109, D168, R171, T246 and I250 residues. To date, canonical eukaryotic and bacterial LDHs crystal structures present a very similar fold with the exception of a 25 amino acid N-terminal extension only presents in vertebrate's enzymes (Clarke et al. 1989, Piontek et al. 1990; Iwata et al. 1994; Auerbach et al. 1998; Read et al. 2001, Chaikuad et al. 2005; Coquelle et al. 2007; Swiderek et al. 2009; Matoba et al. 2014; Ikehara et al. 2014; Kolappan et al. 2015; Friberg et al. 2020, Iorio et al. 2022).

Phylogenetic and biochemical studies have revealed that LDHs belong to a large super family of 2-hydroxy acid dehydrogenases that includes also malate dehydrogenases (MDHs) (Madern, 2002, Madern et al., 2004; Boucher et al., 2014). While LDH use pyruvate as substrate, MDH convert oxaloacetate (OAA) into malate. Most recent studies indicate that the capacity to

convert pyruvate into lactate emerged from MDHs several times independently (Madern, 2002; Madern et al. 2004, Boucher et al. 2014; Steindel et al. 2016, Brochier-Armanet and Madern 2021): one event led to the large group of LDHs found in bacteria and in most eukaryotes that are characterized by the presence of a conserved glutamine at position 102 (referred thereafter as to canonical LDH), while four events led independently to the emergence of LDH in *Plasmodium* (*Eucarya, Apicomplexa*), *Cryptosporidium* (*Eucarya, Apicomplexa*), *Trichomonas vaginalis* (*Eucarya, Parabasalia*), and *Selenomonas ruminantium* (*Bacteria, Firmicutes*) (see (Brochier-Armanet and Madern 2021) and references therein). Conversely, a single case of LDH toward MDH activity has been recently documented in *Planctopirus limnophila* (*Bacteria, Planctomycetes*) (Brochier-Armanet and Madern 2021).

In vertebrates, tetrameric LDHs are encoded by three homologous genes, which are expressed in different tissues: LDH-A (encoding a muscle type-specific (M) isozyme), LDH-B (encoding a heart type-specific (H) isozyme), and LDH-C (encoding a testis-specific (C) isozyme) (Goto et al. 2016). The phylogenetic relationships between vertebrate LDH and more generally between metazoan LDH are not well resolved. However, early studies suggest that they derive from bacterial sequences (Stock et al. 1993; Tsoi and Li 1994; Tsuji et al. 1994). Ever since, the number of available sequences has considerably grown allowing to reinvestigate the evolutionary relationships between eukaryotes LDHs, including those from non-metazoan eukaryotes (e.g. plants, fungi), and bacterial LDHs.

Numerous studies have shown that LDHs are relevant model enzymes to study allosteric regulation (Garvie, 1980, Brochier-Armanet and Madern 2021) and references therein). In fact, most of the characterized bacterial LDHs are typical allosteric enzymes, for which the allosteric effector is fructose 1,6-bisphopshate (FBP). In contrast, a single case of non-allosteric bacterial LDH, which is constitutively activated without FBP, has been identified and documented in *Lactobacillus pentosus* (Uchikoba et al. 2002). In the absence of FBP, bacterial allosteric LDHs exhibit a sigmoid pyruvate saturation profiles with a complete lack of activity at physiological low concentration of pyruvate (Arai et al. 2002; Iorio et al. 2021). This corresponds to a typical homotropic activation phenomenon. When the enzymatic reaction proceeds in presence of FBP, the activity profile turns hyperbolic, demonstrating a heterotropic allosteric activation (Schroeder et al. 1988; Arai et al. 2002; Feldman-Salit et al. 2013; Taguchi, 2017). Crystal structures have revealed that residues R173, H188, Y190 (referred as the FBP-binding site (FBP- BS) signature sequence thereafter) located at the P-axis related interface participate to the binding of FBP in allosteric LDHs (Iwata and Ohta. 1993; Iwata et al. 1994; Coquelle et al. 2007).

Allosteric transition of bacterial LDHs fits well the ensemble model of allostery (Motlagh et al. 2014; Nussinov et al. 2014; Guo and Zhou 2016), as well as the classical concerted Monod-Wyman-Changeux (MWC) model, in which the T-inactive and R-active states of enzymes coexist in a pre-equilibrium independently of allosteric effectors (Monod et al. 1965).

Canonical eukaryotic LDHs differ from their bacterial homologues by several aspects. While all the bacterial LDHs occur as homo tetramers, vertebrates LDH may assemble in different ways. In particular, LDH-M and LDH-H can form homo or hetero tetrameric assemblies, whereas, LDH-C form exclusively homo tetramers (Sakai et al. 1987; Read et al. 2001). M and H forms display a marked difference in their respective affinity for pyruvate and their sensitivity to inhibition by high concentration of this substrate (Dawson et al. 1964). The formation of M / H LDH hetero tetramers is thought to play a role in the development of vertebrate embryo (Cahn et al. 1962, Goto et al. 2016). Enzymatic properties of the various forms of vertebrate LDHs indicate an absence of cooperativity between subunits (Pesce et al. 1967; Everse and Kaplan, 1973; LeVan and Goldberg, 1991; Holland et al. 1997). Compared to bacteria, structures from vertebrates LDHs have revealed that the N-terminal extension create additional interactions between subunits (Kolappan et al. 2015 and references therein) and the deletion of this extension in *Homo sapiens* LDH (*H. sapi* LDH) led to a strongly unstable enzyme (Zeng et al. 2004). This structural feature was suggested to be responsible for the absence of allosteric capacity, allowing vertebrate LDHs to continuously exist in an R-active state (Kolappan et al. 2015). However, some studies have demonstrated that such an assumption is no longer valid. In fact, using biophysical and molecular dynamics simulations, it has been shown that the LDH-M from the rabbit displays some reminiscent allosteric properties (Katava et al. 2017). More recently, it has been shown that rabbit and human LDHs -M undergo allosteric transition under mildly acidic conditions (Pasti et al. 2022, Iacovino et al. 2022).

Regarding plants, LDH biochemical studies are rare. However, they display a different behavior compared to vertebrate LDHs. By showing that their enzymatic properties do not follow the Michealis-Menten kinetic, they are considered as homotropically activated enzymes (Betsche 1981; Tihannyi et al. 1989; O'Carra and Mulcahy 1995; Sugiyama and Taniguchi, 1997). Sequence comparison indicates that plant LDHs also exhibit a long N-terminal extension (Hondred and Hanson, 1990) without structural data to date. Data concerning fungi are even rarer. The LDH from *Phycomyces blakesleeanus* (*P. blak* LDH) was shown to harbor both the homo- and heterotropic allosteric activation as bacterial LDH (De Arriaga et al. 1982; Soler et al. 1982). Primary sequence inspection of fungi sequences indicates the N-terminal extension is absent. As in the case of plants, no structural data is available regarding fungi LDH.

Here we investigate the links between canonical LDHs from eukaryotes and their bacterial counterparts using an integrated approach. An in-depth phylogenetic analysis, reveals that in eukaryotes, LDHs have been acquired via two independent horizontal gene transfers (HGT) from bacteria: vertebrates and plants LDHs have been acquired from cyanobacteria, while fungi sequences have been acquired from another bacterial donor. The biochemical and structural characterization of the *Cyanobacterium aponinum* LDH (*C. apon*, *Cyanobacteria*) and the kinetic characterization of the *Rosa chinensis* LDH (*R. chin*, plants), reveal that *C. apon* LDH displays an unexpected mix of bacterial and eukaryotic LDH properties, while the *R. chin* LDH is representative of a strict homotropically activated enzyme. In addition, we characterized a set of *C. apon* LDH mutants designed to specifically alter the allosteric behavior of the resulting enzymes.

This work reveals the scenario by which allosteric regulation capacity in LDHs evolved over the bacterial and eukaryotic Domains.

Material and Methods

Phylogenetic analyses

A recent in-depth analysis of 16,052 reference proteomes from UniProt (https://www.uniprot.org/proteomes/) resolved the relationships between MDH and LDH (Brochier-Armanet and Madern 2021). Starting from this study, we retrieved the 484 canonical LDH sequences identified by Brochier-Armanet and Madern (2021) in a representative and non-redundant sampling of 2,272 proteomes (266 eukaryotes, 269 archaea, and 1,737 bacterial proteomes). We also included the proteome and the LDH sequence of the plant *Rosa chinensis* that is part of the 16,052 reference proteomes but not to be part of the 2,272 proteomes retained by Brochier-Armanet and Madern (2021). So, in total, we considered 2,373 proteomes. We also included four bacterial MDH used as outgroup: the sequence from the alphaproteobacterium *Rhodospirillum centenum* ATCC 51521 (uniprot_id B6IYP5), Chloroflexi *Chloroflexus aurantiacus* ATCC 29366 (uniprot_id P80040), the Chlorobi *Chlorobaculum tepidum* ATCC 49652 (uniprot_id P80039), and the Bacteroidetes *Salinibacter ruber* DSM 13855 (uniprot_id Q2S289). The 489 sequences have been aligned with MAFFT v7.453 (Katho et al. 2013) using the accurate L-INS-i option. The resulting alignment has been trimmed using BMGE v1.2 (Criscuolo and Gribaldo 2010) with the BLOSUM30 substitution matrix. A maximum likelihood (ML) phylogenetic tree has been inferred with IQ-TREE v1.6.12 (Nguyen et al. 2015). The LG+G4 model was identified by ModelFinder (Kalyaanamoorthy et al. 2017)

as the most suitable for the tree reconstruction. Branch supports have been estimated using the ultra-fast bootstrap procedure implemented in IQ-TREE (1,000 replicates).

Tree drawing, residue mapping, and heatmap

Tree figures were drawn with iTOL v5 (Letunic and Bork, 2021)

Protein expression and purification

The *C. apon, R. chin* LDHs genes and various mutants were purchased (GENECUST) and cloned in a pET 20a plasmid for overexpression. A six histidine extension was encoded at the C-terminal part of the resulting constructs. *Escherichia coli* BL21 (DE3) strain transformed with the LDH plasmid were grown in LB medium with ampicillin (100 µg/mL) at 37 °C until OD(600 nm) of 0.5. After a cold shock (4 °C for 5 hrs), IPTG was added to a final concentration of 0.2 mM to induce expression and the culture incubated at 20 °C overnight. Cells were harvested by centrifugation at 5000 g for 30 minutes at 4 °C. The pellet was suspended in 40 mL of buffer 1 (50 mM Tris-HCl pH 7.0, 50 mM NaCl). Prior cells disruption, 5 µg/mL of DNAse (Roche), 10 mM $MgCl_2$, protease inhibitors (Roche) and lysozyme (Roche) were added. The preparation cooled at 4 °C was disrupted by sonication (Branson). The crude extract was then centrifugated at 13 000 g for 30 min at 4 °C, filtered and applied on Nickel affinity column (HiTrap HP 5 mL - GE healthcare) equilibrated in buffer 1. The column was washed with 15 ml of 50 mM Tris-HCl pH 7, 200 mM NaCl, and then by 15 ml of 20 mM Imidazole. The protein was eluted with buffer 1 complemented with 300 mM Imidazole. The fraction was diluted 3 times before being applied to a co-factor affinity column (Blue Sepharose 5 mL - GE Healthcare) equilibrated with buffer 1. A gradient of NaCl (50 mM to 2.5 M) was applied to elute the protein. Fractions containing the purified protein were then concentrated in buffer 2 (50 mM bis-Tris propane pH 6.1, 50 mM NaCl) before a final size exclusion chromatography step (S200 10/300 Increase equilibrated with buffer 2). The pure active fractions in buffer 2 were pooled and concentrated to 20 mg/mL and stored at 4°C. We found buffer 2 was more efficient than buffer 1 for long term stability storage at 4°C.

Size Exclusion Chromatography - Multi Angle Laser Light scattering (SEC-MALLS).

SEC combined with online detection by MALLS and refractometry (RI) was used to measure the absolute molecular mass of proteins in solution. The SEC run was performed using an ENrich^{TM} SEC650 10x300 gel-filtration column (Biorad) equilibrated with buffer 1. Separation was performed at room temperature. 50 µl of the protein stock solution diluted at ~5 mg ml^{-1}

with buffer 1, was injected with a constant flow rate of 0.5 ml^{-1} min^{-1}. Online MALLS detection was performed with a DAWN-HELEOS II detector (Wyatt Technology Corp.) using a laser emitting at 690 nm. Protein concentration was determined by measuring the differential refractive index online using an Optilab T-rEX detector (Wyatt Technology Corp.) with a refractive index increment *dn/dc* of 0.185 ml^{-1} g^{-1}. Weight-averaged molecular weight (Mw) determination was done with the ASTRA6 software (Wyatt Technologies) and curve was represented with GraphPad Prism software.

Analytical ultra-centrifugation.

Ultra-centrifugation experiments were conducted in an XLI analytical ultracentrifuge (Beckman, Palo Alto, CA) using an ANTi-50 rotor, using double channel Epon centerpieces (Beckman, Palo Alto, CA) of 12 mm optical path length equipped with sapphire windows, with the reference channel being typically filled with the solvent of the sample. Acquisitions were done at 20°C and at 42,000 rpm (130,000g), overnight, using absorbance (280 nm) and interference detection. Data processing and analysis was done using the program SEDFIT, and GUSSI using standard equations and protocols (Le Roy et al. 2015).

Standard enzymatic assays.

LDH activity was assessed by measuring the initial rates of PYR reduction (NADH oxidation) at 340 nm in a thermostated spectrophotometer from JASCO. The standard assay mixture contained 50 mM Tris-HCl pH 7.0, 50 mM NaCl, 0.3 mM NADH and various concentration of substrate in a final volume of 0.6 ml. The reaction was initiated by addition of the enzyme. LDH assays were carried out at 35°C. One unit of LDH activity corresponds to the amount of enzyme that catalyzes the oxidation of 1 micromole of NADH per min. The data were analyzed using Graph Pad Prism V6 using the Michaelis-Menten or Allosteric sigmoidal option. The substrate saturation profiles were normalized by the maximal velocity values obtained for each enzymes. With homotropicaly activated LDH, the maximal value considered was in the presence of FBP effector.

Crystallization of *C. apon* LDH

Initial crystallization screening was performed at HTX-lab (EMBL, Grenoble, www.htxlab.embl.fr) as sitting drops in 6 standard screens (The Classics Suite and The Pegs Ions from Qiagen, The JCSG + and the PACT from Molecular Dimensions, Wizard I & II from Rigaku and Salt-Grid derived from Hampton) at 20°C in Crystal Direct plates. Drops were

inspected and scored at different time points for hits over 35 days. Apo and Holo *C. apon* LDH were crystallized in the presence of Crystallophore (TbXo4, https://crystallophore.fr/).

For Apo *C. apon* LDH crystallization, a TbXo4 / *C. apon* LDH mixture (prepared by dissolving TbXo4 powder with *C. apon* LDH at 15 mg/mL for a final TbXo4 concentration of 10 mM) was prepared two hours before setting up the crystallization experiment (100 nL of protein sample then 100 nL of crystallization solution). Crystals were manually reproduced in 24-well plates (Molecular Dimensions) with the condition 17 % Peg MME 550, 0.1 M bicine pH 9.0, 0.1 M NaCl. Hanging drops were setup by adding 1.5 µL of TbXo4 / *C. apon* LDH mixture plus 1.5 µL of reservoir solution. Crystals appeared within few days at 20 °C. Prior data collection, crystals were cryo-protected with a higher Peg MME 550 concentration (22 %) and flash frozen in liquid nitrogen.

The *C. apon* LDH ternary complex was prepared by mixing oxamate (to substitute the LDH substrate), FBP, NADH and *C. apon* LDH at a final concentration of 2 mM for the ligands and 12 mg/mL for the enzyme. The drops were set up using the Xo4-standard protocol as implemented at HTX-lab (addition of 100 nL of protein sample then 100 nL of TbXo4 at 10 mM in 10 mM Sodium bicarbonate and then 100 nL of crystallization solution). Crystals were obtained in Crystal Direct plates with the condition 0.2 M Na malonate dibasic monohydrate, 20 % Peg3350. Crystals appeared overnight at 20 °C. Crystals were automatically harvested with the Crystal Direct harvester and flash frozen at HTX-lab after cryoprotection with glycerol (10 % final concentration).

Apo *C. apon* LDH structure

Diffraction data were collected on the Proxima-1 beamline at Soleil synchrotron at the selenium edge (0.984 Å). Data were treated anomalously with xds (Kabsch, 2010). Structure phasing was performed with Crank-2 (ccp4 suite, Winn et al. 2010) using the anomalous signal from 3 Tb sites. Subsequent refinements were done with coot (Emsley et al. 2010) and refmac (ccp4 suite), images prepared with Pymol (https://pymol.org/2/).

The asymmetric unit contains one *C. apon* LDH molecule, one TbXo4 molecule and three terbium atoms. The relevant biological tetramer is built through crystal symmetry. The TbXo4 molecule is coordinated to E62 and forms further interactions via its picolinate moiety with W218 of a neighboring tetramer.

***C. apon* LDH ternary complex structure**

Diffraction data were collected on the Massif-1 beamline at ESRF synchrotron. The structure was solved by molecular replacement using the *H. sapi* LDH-M structure (PDBID 4OJN) as a model. Subsequent refinements were done with coot and buster (https://www.globalphasing.com/). Structure representations were prepared with Pymol. The asymmetric unit contains one *C. apon* LDH tetramer, in which four oxamate, two FBP and four NADH molecules are bound. No anomalous signal was found indicating the absence of TbXo4 in this structure.

Crystallographic software support was provided by SBGrid (Morin et al. 2013). Data collection and refinements statistics are in Supplementary Table S1.

Results

A new picture of eukaryotic LDHs evolution.

Compared to bacterial enzymes, eukaryotic LDH display different biochemical and structural properties. Our goal was to understand how and when these properties emerged, with a particular emphasis on the allosteric capacity. As a first step, we sought to clarify their evolutionary history and relationships with prokaryotic LDH. An in-depth survey of 2,273 proteomes representative of UniProt reference proteomes led to the identification of 485 canonical LDH sequences present in 438 (19.3%) proteomes (Supplementary Table S2). The ML phylogeny of the 485 LDH sequences is shown as Fig. 1. Mapping experimental data from this work and literature (Table 1) on this tree provides new information that are discussed below. Most of the LDH sequences are present in bacteria (375 sequences in 357 of the 1,737 (20,6%) bacterial proteomes) and in eukaryotes (105 sequences in 77 of the 267 (28.8%) eukaryotic proteomes), while they are rare in archaea (5 sequences in 4 of the 269 (1.5%) archaeal proteomes).

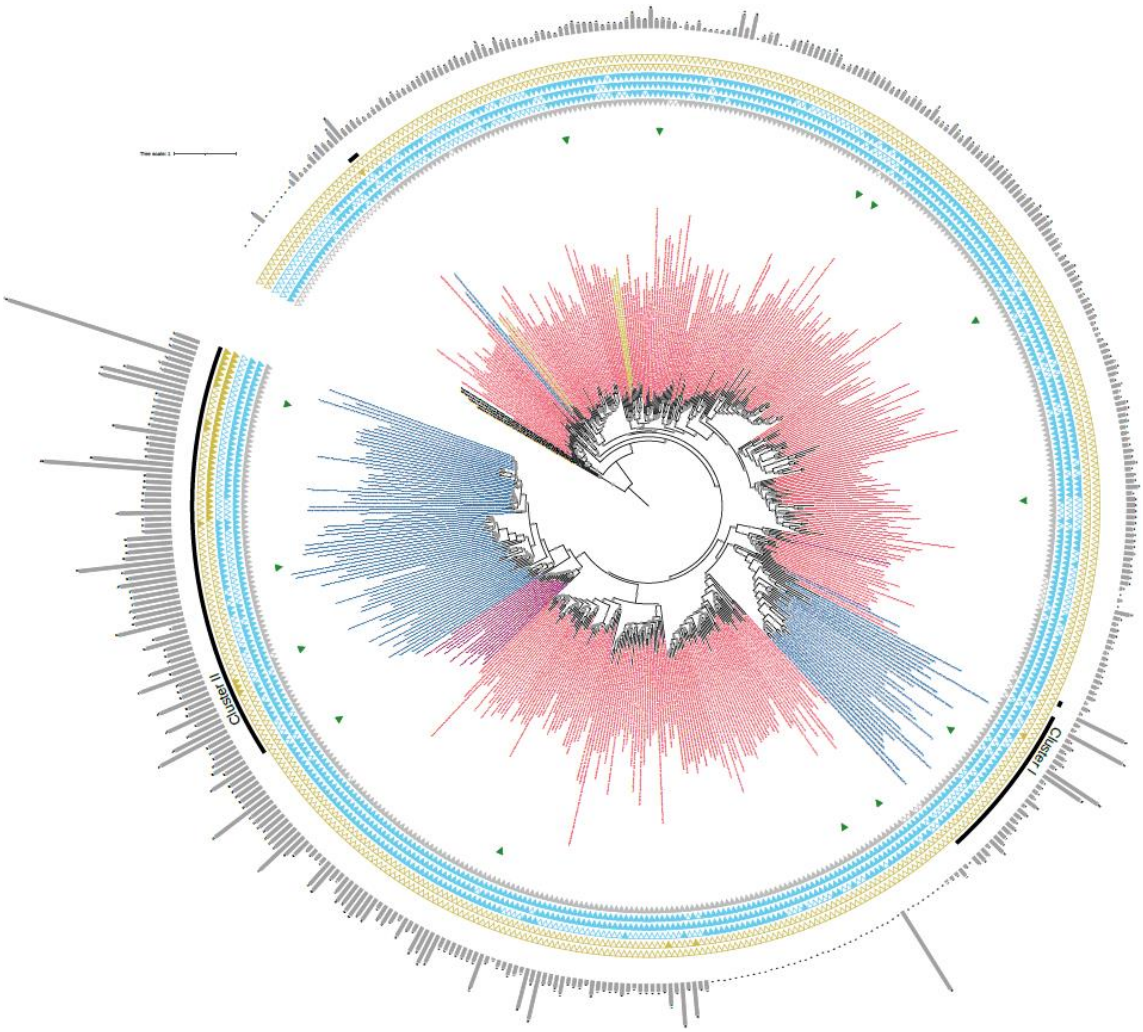

Fig. 1. Rooted maximum likelihood tree of the 485 LDH sequences identified in 2,273 proteomes representative of the taxonomic diversity of Archaea, Bacteria, and Eukarya for which complete proteome sequences are available. MDH sequences used to root the tree are in black. Archaeal LDH are in yellow, bacterial LDH in pink (with cyanobacterial sequences in dark pink), and eukaryotic sequences in blue.
Green triangles designate characterized LDH sequences according to this study or literature (see also Table 1). From the innermost to the outermost circle, filled triangles correspond to: (i) the presence of Q102 (Grey), the critical residue involved in pyruvate recognition, (ii-iv) three major residues involved in FBP binding (R173, H188, and Y190, in blue), and (v-vi) two histidine that participate to the LDH tetrameric assembly (H183 and H218, olive), while empty triangles indicate the presence of other residues. The presence of the N-terminal extension is shown by grey rectangles of various size. The scale bar corresponds to the average number of substitutions per amino acid site in the sequences. Grey circles represent the robustness of branches (ultrafast bootstrap, 1,000 replicates). For clarity, only values > 90% are shown. A larger picture of this tree is shown as Supplementary Figure S1.

The very narrow distribution of LDH in archaea suggests that they have been acquired by HGT and not by vertical inheritance from the common ancestor of all archaea. Strengthening this hypothesis, archaeal LDH are mixed with bacterial sequences and do not form a monophyletic group in the LDH phylogeny (Fig. 1 and Supplementary Figure S1), indicating independent

acquisitions from different bacterial donors. For eukaryotes a similar situation is observed, as eukaryotic sequences are not grouped together in the tree, which suggests again several and independent origins. More precisely, eukaryotes LDH emerge at three different positions (Figs. 1 and 2). Two fungi sequences are isolated from the others and group with two archaeal and two bacterial sequences (Bootstrap Value (BV) = 96%). Other eukaryotes sequences form two separated clusters. The smallest (cluster I) gathers sequences from Fungi and one sequence from a member of *Rhizaria* (Figs. 1 and 2), and robustly grouped with a mix of bacterial sequences from various phyla (BV = 97%, Figs. 1 and 2).

The largest group (cluster II) contains sequences of *Metazoa* (including the three human LDH), Plantae (represented here by *Viridiplantae* and *Rhodophyta*), one *Alveolata*, and one *Filasterea* (Fig. 2). Surprisingly, LDH relationships within cluster II show discordance with the phylogeny of eukaryotes. For instance, metazoan sequences are not monophyletic and form three distinct groups: group I gathers sequences from *Spiralia* and *Ciona*, group II from *Ecdysozoa* and *Cnidaria*, and group III from *Vertebrata* (Fig. 2). Determining whether these discrepancies are the result of tree reconstruction artefacts, lack of phylogenetic signal, gene transfers, or hidden paralogies would require dedicated analyses that are beyond the scope of this study. Cluster II is robustly nested within a clade of *Cyanobacteria* (BV = 100%, Fig. 1, purple sequences). The split of eukaryotic sequences in two separated clusters indicated clearly two distinct origins and likely two acquisitions through HGT from distinct bacterial donors. Regarding cluster II, a mitochondrial or archaeal origin, as expected according to the evolutionary history of eukaryotes (Dacks et al. 2016), can be excluded since no link to alphaproteobacterial or archaeal sequences is observed (Fig. 1). In fact, an acquisition from *Cyanobacteria* appears likely, since eukaryotes cluster II sequences are nested within cyanobacterial sequences. In contrast, the situation is less clear for cluster I (fungal and rhizarial sequences), because a few alphaproteobacterial LDHs branch in the vicinity of eukaryotic sequences (Fig. 1). However, these alpha-proteobacterial sequences are mixed with sequences from other bacterial phyla, making the exact origin of cluster I sequences difficult to determine. The relationship between cluster II and cyanobacterial LDH sequences is unexpected because, beside endosymbiotic gene transfers linked to the chloroplast acquisition, ancient HGT from *Cyanobacteria* toward eukaryotes seems to be rare (Rochette et al. 2014). Yet, this relationship was likely not artefactual because it was supported by very high BV (>90%), and the presence of a cysteine at position 35 shared exclusively by cyanobacterial LDH and most of their eukaryotic relatives. In order to link information gained from the phylogenetic analysis with experimental functionality, we investigated the properties of LDHs from two cyanobacteria: *Cyanobacterium*

aponinum (*C. apo*) and *Cyanobium gracile* (*C. grac*), one plant, *Rosa chinensis* (*R. chin*), and one group I metazoan, *Echinococcus granolus* (*E. gran*). Unfortunately, we did not succeed to refold properly the recombinant *C. grac* and *E. gran* LDHs.

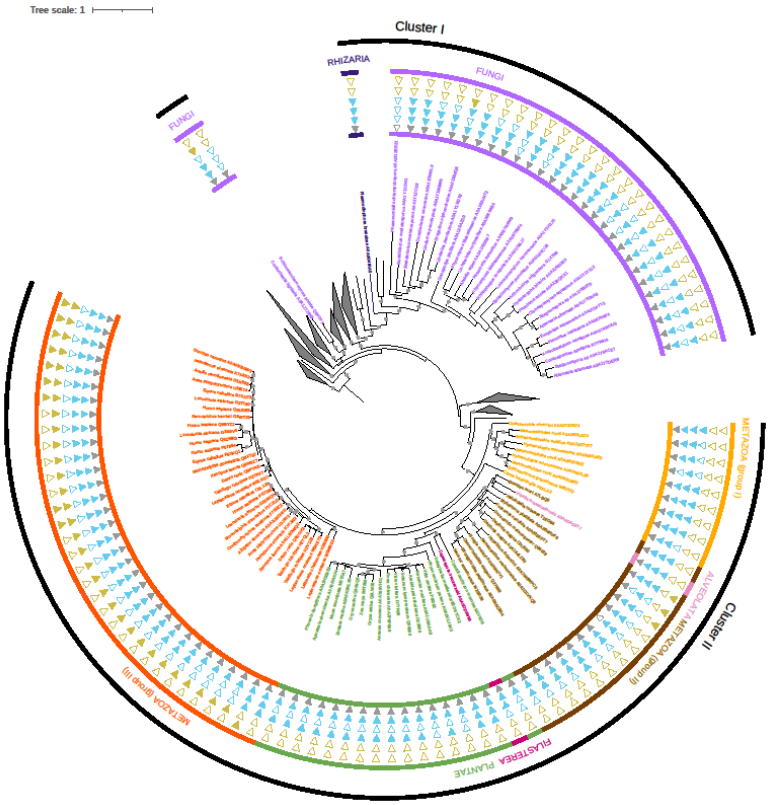

Fig. 2. Focus on the eukaryotic sequences of the maximum likelihood tree shown on Fig. 1. For clarity prokaryotic sequences have been collapsed. Colours represent taxonomic groups: light pink corresponds to *Alveolata*, dark pink to *Filasterea*, green to *Plantae*, purple to *Fungi*, yellow to *Metazoa* group I (*Spiralia* and *Ciona*), brown to *Metazoa* group II (mainly *Ecdysozoa* and *Cnidaria*), and orange to *Metazoa* group III (Vertebrata).
Green triangles designate characterized eukaryotic LDH sequences according to this study (*Rosa chinensis*) or to the literature (the metazoan *Homo sapiens* and the fungi *Phycomyces blakesleeanus*). From the innermost to the outermost circle, filled triangles correspond to: (i) the presence of Q102 (Grey), the critical residue involved in pyruvate recognition, (ii-iv) three major residues involved in FBP binding R173, H188 and Y190 (Blue), and (v-vi) two histidine that participate to the LDH tetrameric assembly (H183 and H218, olive), while empty triangles indicate the presence of other residues. The scale bar corresponds to the average number of substitutions per amino acid site in the sequences. Grey circles represent the robustness of branches (ultrafast bootstrap, 1,000 replicates). For clarity, only values > 90% are shown. A larger picture of this tree is shown as Supplementary Figure S1.

Allosteric activation capacity of *C. apon* LDH

We measured enzyme kinetics of recombinant *C. apon* and *R. chin* LDHs and compared the data with those published for the canonical allosteric bacterial LDH of *Bifidobacterium longum* (*B. long*, *Actinobacteria*), an enzyme devoid of any N-terminal extension as all bacterial LDHs, except the cyanobacterial ones, and the vertebrate non-allosteric M- and H-LDHs (Fushinobu et al. 1996; Vesell 1965; Wuntch et al. 1970). However, accurate comparisons with data from the literature are difficult because kinetic measures are not uniform. To overcome this issue, we present "normalized" substrate saturation profiles recorded at pH 7 in percentage of the maximal activity obtained for each enzyme of this study and from the literature. This allows to visualize and investigate (i) pyruvate affinity changes and (ii) allosteric properties from the shape of the substrate saturation profile. Indeed, a sigmoid activity profile using pyruvate as substrate, indicate that the allosteric LDHs are found in an equilibrium between two states, a low affinity T- and high affinity R- states in the absence of allosteric effectors. In presence of FBP, the equilibrium is displaced toward the R-state and becomes hyperbolic.

Without any effector, the *B. long* LDH saturation profile is typical of homotropic activation with a sigmoid shape (Fig. 3A). When the reaction mixture is supplemented with 0.1 mM of FBP, the enzyme is strongly activated with an increase in maximal activity and a strong shift of pyruvate affinity toward low values (Fig. 3A). The corresponding curves are typical of allosteric behaviour, with both homotropic and heterotropic activation, as observed for bacterial LDHs devoid of N-terminal extensions, such as the LDH from *Thermus* species (Taguchi 2017).

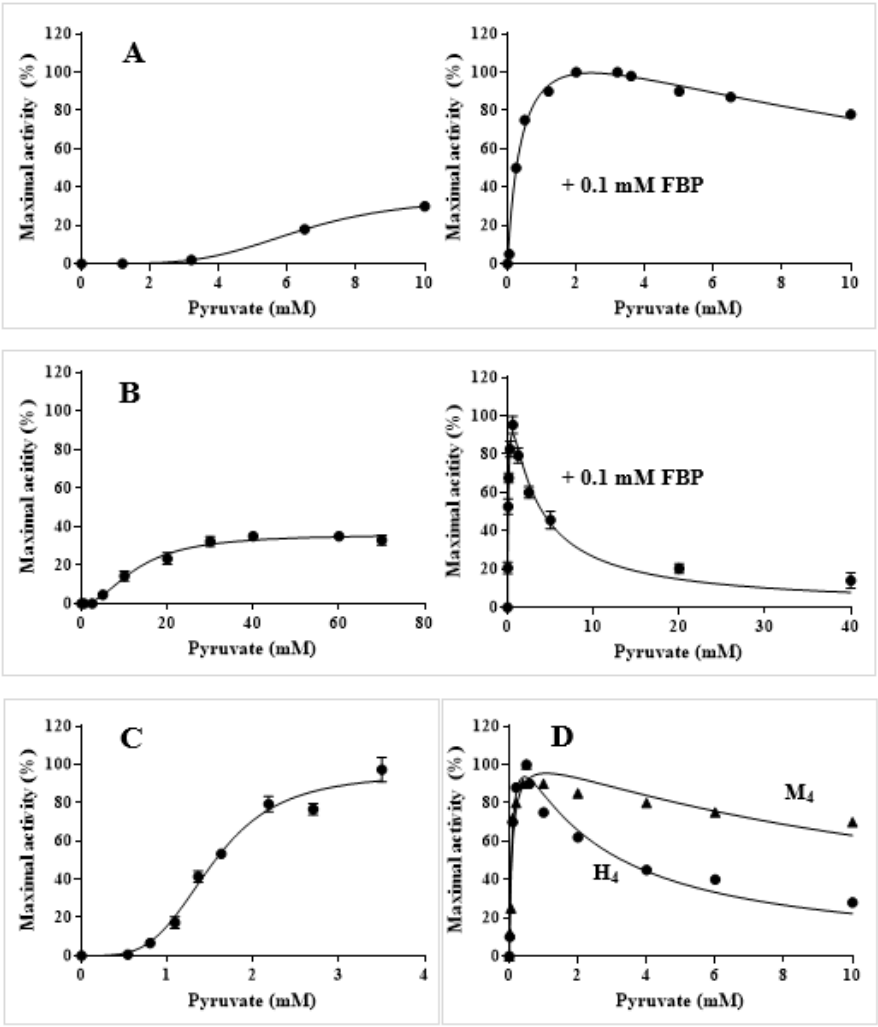

Fig. 3. Pyruvate saturation curves of four LDHs. Measurements were done in the presence of the indicated concentrations of pyruvate with NADH as coenzyme. (A) *B. long* LDH, without or with FBP, left and right panels, respectively. Data from (Fushinobu et al. 1996). (B) *C. apon* LDH, without or with FBP, left and right panels, respectively. (C) *R. chin* LDH without FBP. (D) Human muscle (M4-LDH) and heart (H4-LDH). Data from (Vesell 1965).

Then, we investigated the properties of the *C. apon* LDH, a cyanobacterial enzyme with a long N-terminal extension, closely related to cluster II eukaryotes LDH. Unexpectedly, the pyruvate saturation profile of *C. apon* LDH is also sigmoid (Fig. 3B), as in *B. long* (Fig. 3A), with a K_m value for pyruvate of 10 mM, despite the presence of an N-terminal extension. In the presence of FBP, the enzyme of *C. apon* (Fig. 3B) behaves again like that of *B. long* (Fig. 3A), as the maximal enzymatic activity increases and the affinity is shifted toward low concentration of substrate, with a K_m value for pyruvate of 0.1 mM. In the presence of FBP, the *C. apon* LDH is sensitive to inhibition by high concentration of substrate (Fig. 3B), as it is frequently encountered in LDHs (Eszes et al. 1996). When FBP is added, the enzyme turnover (k_{cat}) is

increased from 46 s^{-1} to 182 s^{-1} (Table S3). The FBP exerts therefore a strong favorable activation effect on the *C. apon* LDH. We continued our investigation by analyzing the *R. china* LDH, a plant enzyme with a long N-terminal extension, belonging to cluster II eukaryotes LDH. Here again, the *R. china* LDH enzymatic activity profile is sigmoid (Fig. 3C). The K_m value for pyruvate is 1.5 mM with a k_{cat} value of 110 s^{-1} (Table S3). We tested whether the addition of FBP influences and found no significant effect on activity (data not shown). Therefore, the *R. china* LDH shows only homotropic activation. The typical profile saturation curves of *H. sapi* LDHs (M and H forms) display neither sigmoid activation profile nor activation by FBP (Fig. 3D), as expected for non-allosteric enzymes (Vesell, 1965). Such a behavior holds also when Pig and Rabbit LDHs are investigated (Wuntch et al. 1970).

Our data found with *R. chin* and *C. apon* LDHs as representative enzymes, indicated that plants and cyanobacterial LDHs shared a homotropic capacity, nonetheless heterotropic activation is absent in this plant. These findings challenge the proposed role of N-terminal extensions as a structural element unfavorable for allosteric regulation.

Distribution of allostery in LDHs.

To go further, we decided to add our data to those from the existing literature. The resulting table allows to present a survey of functional and regulatory properties of 14 LDHs, 2 from this work and 12 from the literature (enzymes 3 to 16 in Table 1). When analyzed with respect to the phylogeny of LDHs, it brings new insight on the evolution of allosteric behavior of these important enzymes. We recall that in the outgroup, tetrameric MalDHs, exemplified here by *C. aura* and *P. limn* (enzymes 1 and 2 in Table 1, respectively), are non-allosteric and display hyperbolic substrate saturation profiles (Rolstad et al 1988; Brochier-Armanet and Madern 2021). The 14 LDHs are widespread across the LDH phylogeny and belong to various bacterial and eukaryotic species (Figs. 1 and 2). As expected, they recognize pyruvate as substrate and display Q102, a residue considered as strong signature for LDH functionality (see (Brochier-Armanet and Madern 2021) and references therein). The distribution of properties shows allostery is a dominant phenotype of LDHs (Figs. 1 and 2). In fact, to the exception of the LDHs from *L. pent* and *S. aure* (enzymes 5 and 8, respectively), other bacterial and the fungal LDHs (3, 4, 6, 7, 9, 10, 11, and 12) are both homotropically and heterotropically controlled by pyruvate and FBP (Table 1, Figs. 1 and 2). Furthermore, we noticed that in the part of the LDH tree encompassing these enzymes, the FBP-BS signature sequence is prevailing. The crystal structure of the tetrameric LDH of *L. pent* (enzyme 5) has shown that the lack of allosteric regulation is due to a strong stabilizing interaction at the AB-like interfaces, which maintains

the enzyme in the R-active state and prevents its ability to explore the T-state (Uchikoba et al. 2002). Consistently, because there is no regulation by FBP in this enzyme, the three amino acids involved in FBP binding are absent. In the case of *S. aure* LDH (enzyme 8), to our knowledge there is no structural information explaining its behaviour.

Regarding eukaryotic LDHs, the situation is different. Available data show differences between clusters I and II that make sense with two distinct origins. In cluster I, the *P. Blak* LDH displays both homo- and heterotropic activations (De Arriaga et al. 1982; Soler et al. 1982) and the FBP-BS signature (Table 1), but not the long N-terminal extension observed in cluster II eukaryotic LDHs. These features are shared with enzymes from *Deinococcus radiodurans* and *Thermus thermophius* (enzymes 10 and 11) (Coquelle et al. 2007), two bacterial LDHs related to cluster I (Supplementary Figure S1). In contrast, eukaryotic LDHs of cluster II and their cyanobacterial relatives (enzymes 13 to 16) harbour an N-terminal extension of 20 to 40 amino acids (Fig. 2 and Supplementary fig. 2), the longest extensions being found in plant LDHs, which display different allosteric features. In fact, we showed that *C. apon* (enzyme 13) is both homotropically and heterotropically regulated as other bacterial LDHs, *R. chin* (enzyme 14) is only homotropically regulated, while *H. sapi* (enzymes 16; LDH-M) is homotropically regulated exclusively at low pH and *D. mela* (enzyme 15) is not allosterically regulated. The dogma suggesting that N-terminal extensions are unfavourable structural features for allostery in LDHs is thus no longer valid.

					Allostery		FBP-BS Signature			
	Organism (taxonomy)	**Code**	**N-term**		**Homo**	**Hetero**	**R173**	**H188**	**Y190**	**UniProt Id**
1	*Chloroflexus aurantiacus* (*Bacteria, Chloroflexi*)	*C. aura*	-	**M**	-	-	**R**	***N***	***C***	P80040
2	*Planctopirus limnophila* (*Bacteria, Planctomycetes*)	*P. limn*	-	**M**	-	-	**R**	***D***	***T***	D5SXK9
3	*Hungateiclostridium thermocellum* (*Bacteria, Firmicutes*) (*Bacteria, Firmicutes*)	*H. ther*	-	**L**	+	+	**R**	**H**	**Y**	Q8KQC4
4	*Moorella thermoacetica* (*Bacteria, Firmicutes*)	*M. ther*	-	**L**	+	+	**R**	**H**	**Y**	Q2RHG3
5	*Lactobacillus pentosus* (*Bacteria, Firmicutes*)	*L. pent*	-	**L**	-	-	**R**	***D***	**Y**	P56512
6	*Lacticaseibacillus paracasei* (*Bacteria, Firmicutes*)	*L. para*	-	**L**	+	+	**R**	**H**	**Y**	Q034V0
7	*Enterococcus mundtii* (*Bacteria, Firmicutes*)	*E. mund*	-	**L**	+	+	**R**	**H**	**Y**	V5XPB8
8	*Staphylococcus aureus* (*Bacteria, Firmicutes*)	*S. aure*	-	**L**	-	-	**R**	***D***	***Q***	Q2G218
9	*Phycomyces blakesleeanus* (*Eucarya, Fungi*)	*P. blak*	-	**L**	+	+	**R**	**H**	**Y**	A0A167R5F4
10	*Deinococcus radiodurans* (*Bacteria, Deinococcus-Thermus*)	*D. radi*	-	**L**	+	+	**R**	**H**	**Y**	P50933
11	*Thermus thermophilus* (*Bacteria, Deinococcus-Thermus*)	*T. ther*	-	**L**	+	+	**R**	**H**	**Y**	Q5SJA1

12	*Bifidobacterium longum* (*Bacteria, Actinobacteria*)	*B. long*	-	**L**	+	+	**R**	**H**	**Y**	P0CW93
13	*Cyanobacterium aponinum* (*Bacteria, Cyanobacteria*)	*C. apon*	+	**L**	+	+	**R**	**H**	**Y**	K9Z684
14	*Rosa chinensis* (*Eucarya, Viridiplantae*)	*R. chin*	+	**L**	+	-	**R**	***Q***	**Y**	A0A2P6P899
15	*Drosophila melanogaster* (*Eucarya, Metazoa*)	*D. mela*	+	**L**	-	-	**R**	**H**	***W***	Q95028
16	*Homo sapiens* (*Eucarya, Metazoa*)	*H. sapi*	+	**L**	Low pH	-	**R**	**H**	***W***	Q9UDE9

Table 1. Functional information and properties of 16 enzymes characterized in this work or from the literature. The presence (+) or absence (-) of the N-terminal extension is indicated in the N-term column. Functionality of the enzymes is reported as M for Malate dehydrogenase or L for Lactate dehydrogenase. The Allostery columns report the existence (+) or absence (-) of homotropic activation (Homo) and heterotropic activation (Hetero). With respect to heterotropic activation: Amino acid variability in the canonical FBP-binding site (FBS-BS) signature are shown in italic. Residue numbering matches the one from Eventoff et al. 1977 and Uniprot numbers are shown in the last column. References: (1) (Rolstad et al 1988), (2) (Brochier-Armanet and Madern 2021), (3) (Ozkan et al. 2004), (4) (Iwasaki et al. 2017), (5) (Taguchi et al. 1992), (6) (Arai et al. 2010), (7) (Matoba et al. 2014), (8) (Yeswanth et al. 2013), (9) (De Arriaga et al. 1998), (10,11) (Coquelle et al. 2007), (12,13) This work, (14) (Karvountzi et al. 1995), (15) (Pasti et al. 2022), and (16, LDH-M) (Dempster et al. 2014). In human, the three LDH forms display the same signature sequence for FBP.

Apo and Holo *C. apon* LDH crystal structures.

To get further insights into the relationship between N-terminal extensions and allosteric behavior, we have solved the structures of both T- and R- states of *C. apon* LDH.

Apo *C. apon* LDH crystal structure was solved by phasing using the anomalous signal of the Terbium cation from the Crystallophore, a metallo-organic complex used as nucleating and phasing agent (Engilberge et al. 2017). Apo *C. apon* LDH tetrameric arrangement agrees with the canonical LDHs "dimer of dimers" structures (named here dimers A//B and C//D) (Coquelle et al. 2007, Friberg et al. 2020), with the formation of four active sites, each of them being able to bind one pyruvate molecule, along with a NADH binding site in the Rossmann-like motif, and two FBP-BSs located at the interface between the two dimers (Fig. 4A). The latest interface is described hereafter as to the AD-like interface. Indeed, because of the crystallographic symmetry, AD and BC interfaces are equivalent. No substrates are bound to the Apo *C. apon* LDH leaving the MbL (residues 101-106) open. As observed in crystal structures of LDHs or

MDHs (Talon et al. 2014), there is a large solvent accessible cavity (SAC) located in between the dimer of dimers that makes the tetrameric assembly.

The *C. apon* LDH ternary complex crystal structure (Holo) was solved by molecular replacement using a *H. sapi* LDH-M as search model (Dempster, et al. 2014) as significant conformation changes between the Apo and Holo *C. apon* LDH prevented to find the molecular replacement solution from the Apo *C. apon* LDH structure. The *C. apon* LDH ternary complex is similarly tetrameric with the co-factor and active sites of each monomer occupied with a NADH and an oxamate molecule inducing the closure of the MbL (Fig. 4B). As expected, two FBP molecules are found in the FBP-binding sites at the AD-like interface.

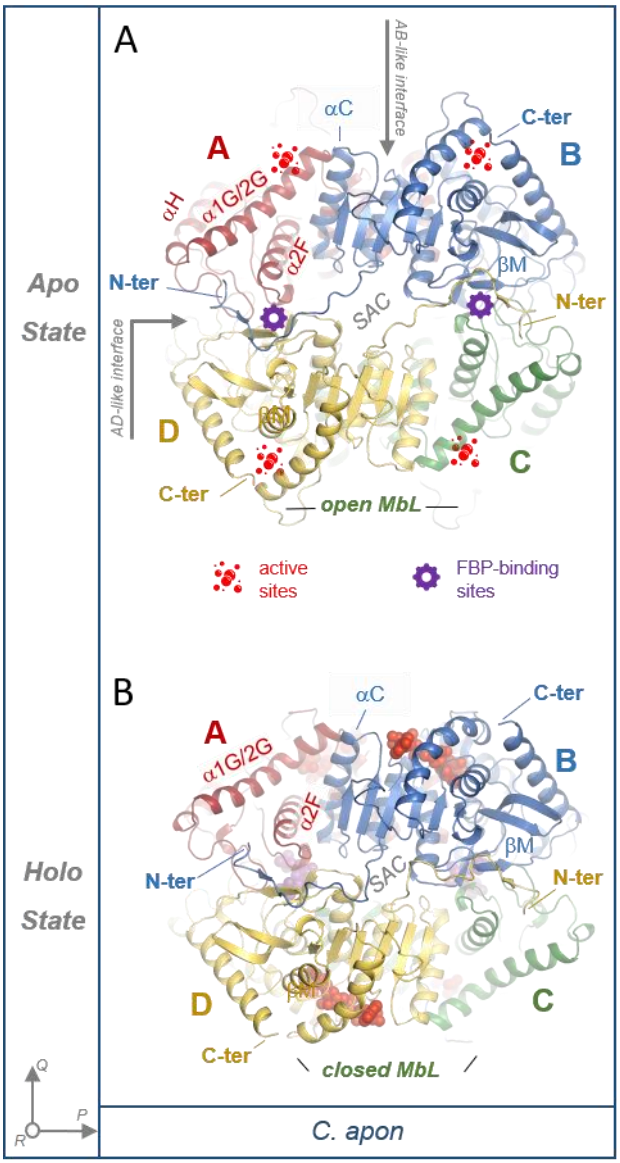

Fig. 4. Ribbon drawing of *C. apon* LDH crystal structure in Apo and Holo states. (A) The Apo state of *C. apon* LDH assembly is a tetramer with four active sites (red bubbles) organized as two functional dimers (A//B and C//D, respectively in red-blue and green-yellow). Two FBP-binding sites (purple wheels) are found at the AD-like interfaces. The N terminal extensions complete the interactions within the tetramer with, for instance, the N-terminal extensions of

monomer B interacting with monomers A and D. AB- and AD-like interface position is indicated as grey arrows. (B) The Holo state of *C. apon* LDH contains four oxamate and NADH molecules (shown as red spheres) and the two FBP-binding sites are filled up with FBP molecules (showed as purple spheres). The tetramer is represented along the *R*-axis according to the conventional definition for LDHs (*P*, *Q* and *R* axis). Position of the mobile loop (MbL) is indicated on both models. SAC corresponds to the solvent accessible cavity.

The fine description of conformation changes between the Apo and Holo states in allosteric LDHs (without any N-term extensions) is well documented (see (Taguchi 2017) for review). *C. apon* LDH undergoes similar conformational changes with local changes induced by substrate and FBP binding impacting the tertiary and quaternary structures of the tetramers. Therefore, we will compare *C. apon* LDH crystal structures with bacterial and eukaryotic LDHs of *B. long* LDH (apo and T-inactive state: pdb ID 1LLD; R-active state: pdb ID 1LTH, chain R) and *H. sapi* LDH-M (Apo: pdb ID 4L4R, ternary complex: pdb ID 4OKN), respectively, into an evolutionary perspective.

Role of N-terminal extensions of *C. apon* LDH folding

The driving point for getting structural information on *C. apon* LDH was to determine the position of its N-terminal extensions and in particular whether they match the position of the N-terminal extensions as described in vertebrate LDH structures. α-carbon representations are shown in Fig. 5.

For the description of the structural differences in the N-terminal extensions, we use the linear structural numbering accordingly to PDB coordinates for each enzyme. To help the reader, a sequence alignment is presented in Supplementary Fig. S3.

In the allosteric *C. apon* LDH, the N-terminal extension of one monomer (*i.e.* B) interacts with two other monomers (A and D in that example) (Fig. 4 and 5B), by creating two area of contacts that are absent in allosteric LDHs lacking the N-terminal extension. In *C. apon*, amino acids N9 to R21 of monomer B interact with monomer D, while amino acid F2 to S8 favors the creation of a "staple-like" element (SLE) between monomers A and D that reinforces AD-like interactions by a grafting process. In fact, in the SLE, residues F2 to I5 form a short helix (αA) allowing the two hydrophobic residues, F2 and I5, to dive into a hydrophobic pocked located in between α1G/2G helix of monomer A and β sheet (βM) of monomer D (Fig. 5 B). The hydrophobic pocket is part of the allosteric core (AlCo), a structural feature involved in the signal communication between LDH monomers (Supplementary Fig. 4) (Taguchi 2017; Iorio et al. 2021). The other extremity of SLE (L6, L7, and S8) makes a short β-sheet (β+), which completes the β-sheet motif (βK, βL, βM) of monomer D, resulting in a supra molecular layer

of these secondary structure elements. Two interfaces (AD-like and BD-like) that contribute to the tetrameric scaffold are thus strengthened by the presence of extensions whereas the AB-like interface is not.

Interestingly, the positioning of the N-terminal extensions in *H. sapi* LDH-M is very similar with the minor difference that hydrophobic residues (L3 and L7) of the short first helix enters deeper in the hydrophobic pocket (Fig. 5C). It has been reported that in Heart *H. sapi* LDH the eight first residues of the N-terminal extensions, with in particular residues L3 and L7, are responsible for tetramerization (Thabault et al. 2020).

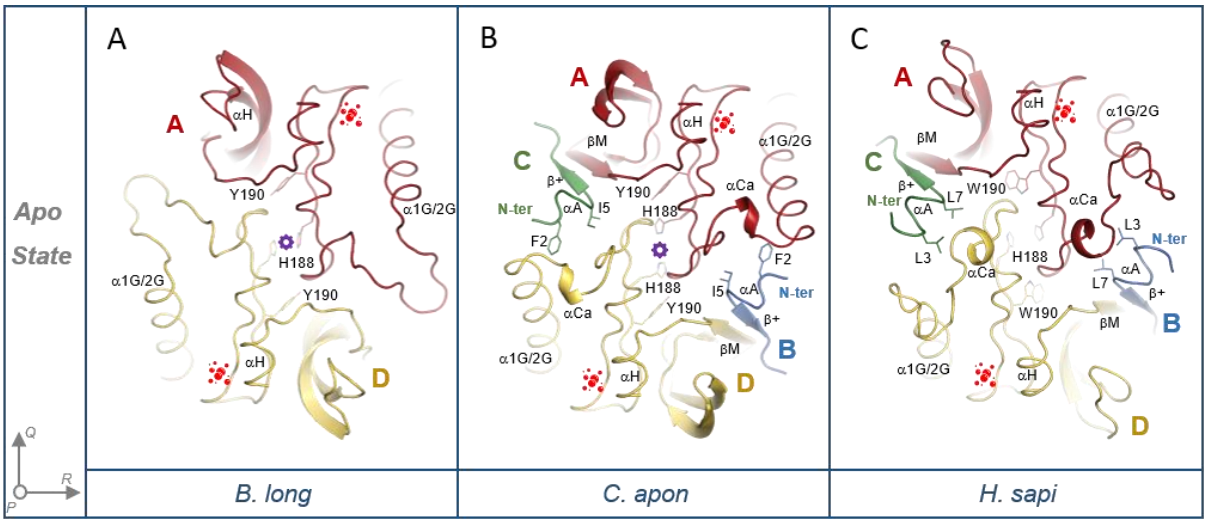

Fig. 5. Comparison of the FBP-binding site and N-terminal extensions in *C. apon* LDH with representative allosteric and non-allosteric Apo LDHs. (A) *B. long* LDH (allosteric), (B) *C. apon* LDH (allosteric, this work). (C) *H. sapi* LDH (non-allosteric) as Apo proteins. Structures are represented along the *P*-axis for observation of the FBP-binding sites (purple wheel in *B. long* LDH and *C. apon* LDH) and the N-terminal extensions (in *C. apon* LDH and *H. sapi* LDH). Monomers are colored as on Fig. 4. To the exception of amino acid of the N-terminal extension (blue and green), the positions are normalized with respect to LDH nomenclature (Eventoff et al. 1977).

In the case of *B. long* LDH, no extensions are present to bring closer monomers A and D. Consequences are the absence of βM (on monomer D) and the lack of constraints on the loop before α1G/2G that adopts a relaxed conformation (Fig. 5A). While the N-terminal extensions of *C. apon* and *H. sapi* LDH-M differ in length and sequence, they share similar conformation and equivalent structural stabilizing features. We next analyzed the amplitude of conformational change frequently encountered in allosteric LDHs.

The active site of *C. apon* LDH samples the T- and R-states.

Based on structural studies of vertebrate LDHs, it is thought that the T-R conformational equilibrium is completely shifted toward the R-active state, independently of the presence of ligands, because of additional interactions between monomers due to N-terminal extension (Abad-Zapatero et al. 1987; Read et al. 2001; Nowicki et al. 2016). The sigmoidal pyruvate saturation profile of *C. apon* LDH suggested that the enzyme can sample the T-inactive state despites the presence of N-terminal extension. So we performed a structural analysis (Fig. 6) of the *C. apon* LDH catalytic site using the Apo and Holo crystal structures, with a special emphasis on the substrate-binding residue R171 for which the side chain position is a relevant structural proxi for T- or R-states in LDHs (Coquelle et al. 2007; Colletier et al. 2010; Tagushi 2017; Iorio et al. 2021).

In Apo *C. apon* LDH (no oxamate bound), the active site R171 residue points to the outside of the protein (OUT position) (Fig. 6B). In order to bind oxamate, rearrangements of helices αC, α2F and α1G/α2G of *C. apon* LDH need to happen, so R171 can move in the active site (IN position) (Fig. 6B). R171 exchanges position with H68 from the adjacent monomer. Indeed, In LDHs, H68 and R171 are neighboring residues with anti-coordinated side chain conformations. When H68 is in the conformation observed in the T-state structure, it prevents the side chain of R171 from accessing the active site and adopting the favorable configuration that binds the substrate analog, oxamate (Coquelle et al. 2007; Colletier et al. 2010; Tagushi 2017, Iorio et al. 2021. Despite the presence of N-terminal extension, the catalytic site of *C. apon* LDH samples T and R- states as observed in *B. long* LDH structures taken as representative of allosteric structural reorganisation. (Fig. 6 A). Catalytic site of *C. apon* LDH differs therefore, from the one in the *H. sapi* Apo LDH-M structure, in which the R171 side chain is described as IN, pointing towards the active site, showing the enzyme is in the R-active state (Fig. 6C). In fact, with *H. sapi* LDH-M the active site is in a pre-competent state for catalysis with H195 and R171 ready to receive a pyruvate molecule that will trigger the closure of the MbL via interaction with Q102 (Fig. 6C).

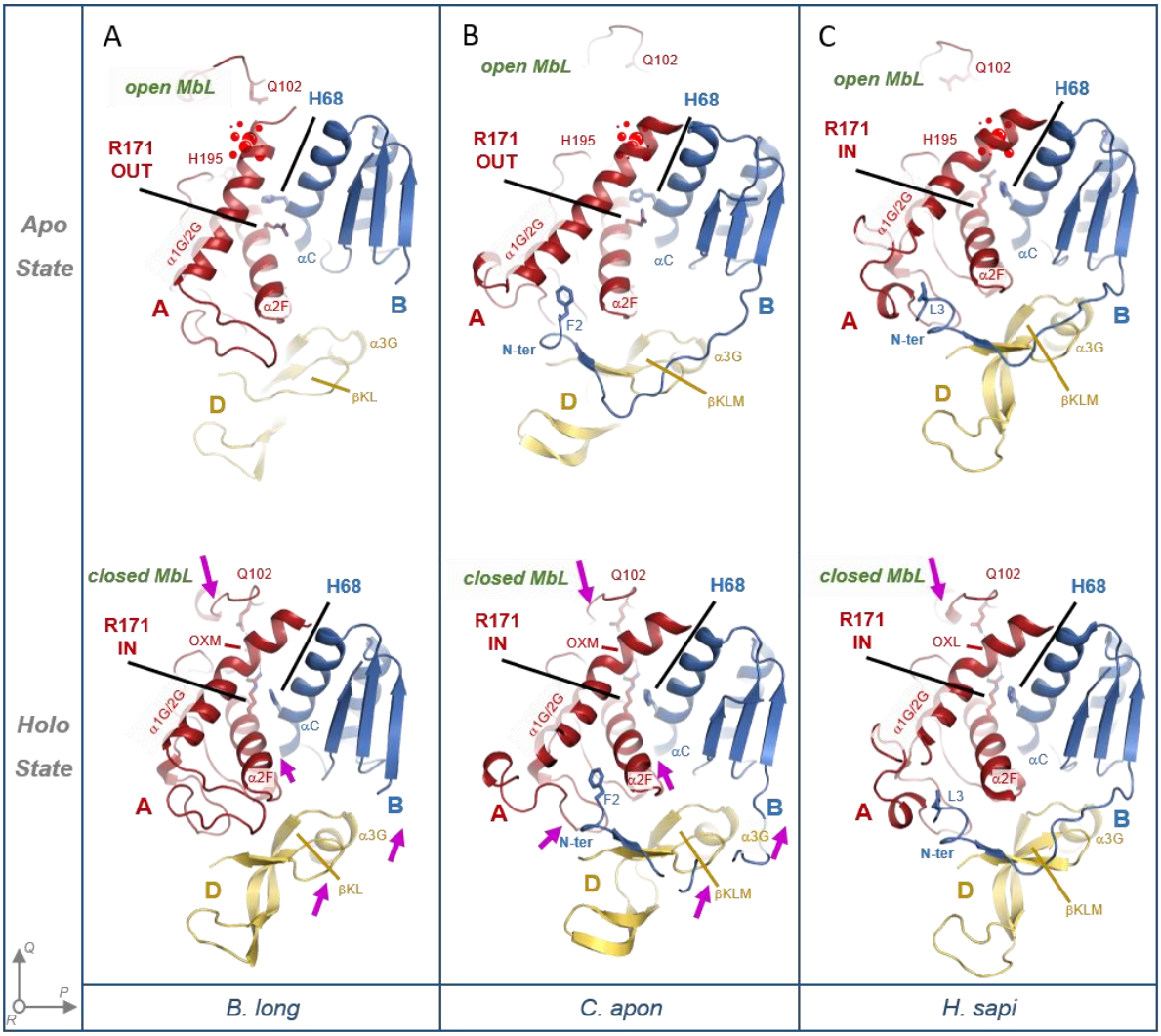

Fig. 6. Detailed view of R171 and the formation of the active site in LDHs. A) *B. long* LDH, B) *C. apon* LDH and C) *H. sapi* LDH-M with comparison of the unbound and bound forms. The side chain position of R171 (OUT or IN position) is indicated. H68 from the adjacent monomer is also indicated. The purple arrows represent the movement of domains when substrates bind. It is worth noting monomer D (yellow) getting closer to monomer B (blue) and the closure of the MbL being similar for the 3 enzymes when substrate binds. The partial view of the tetramers is represented along the *R*-axis. αC helices from monomer B of all models were superposed to generate this detailed view. Monomers are colored as in Fig. 4. The location of the substrate analog oxamate (OXM) in the different Holo states is indicated.

We thus present here an unexpected sampling capacity of *C. apon* LDH between the T-inactive and R state conformation as for bacterial LDHs despite the presence of N-terminal extensions as in eukaryotic LDHs. We next analyzed the amplitude of conformational change frequently encountered in allosteric LDHs.

Large conformational changes upon ligand binding.

First, we analyzed, the consequences of ligand binding on *C. apon* LDH N-terminal extensions. Upon binding of substrates, the enzyme undergoes several rearrangements as observed in the allosteric *B. long* LDH (Iwata and Ohta 1993; Iwata et al. 1994), with the closure of the MbL, the movement of α2F helix, and the bending of α1G/2G helix to reach the R-active state (Fig. 6A-B). The binding of FBP helps the movement of α2F helix by triggering the switch of the R171 position from OUT to IN (Fig. 6A-B). In the case of *C. apon* LDH, the movement of α2F helix and α1G/2G helix increases the size of the hydrophobic pocket below α1G/2G helix and allows the hydrophobic residues of the N-terminal extensions to enter deeper in it. In this sense, the *C. apon* LDH R-active state resembles to the one of *H. sapi* LDH-M (Fig. 6B-C). Secondly, we evaluated the overall reorganization of the tetramer upon binding of substrates. The additional movements in *B. long* and *C. apon* LDHs (see purple arrows in Fig. 6) drag along the β-sheet motif (βKLM) and α3G helix of i.e. monomer D toward the opposite A//B dimer inducing further contacts within the tetramer. These interactions correspond to those existing in *H. sapi* LDH-M (Fig. 6). Moreover, in *B. long* and *C. apon* LDHs the movements have a longer-range impact on the compaction of the tetramer. While Apo or complexed *H. sapi* LDH are mostly found in a compact form, *B. long* and *C. apon* LDHs are breathing between the open T-inactive state and the compact R-active form (Fig. 7). When NAD, FBP and oxamate bind to *B. long* LDH, the tetramer compacts and the access to the SAC decreases.

An open assembly is necessary for the diffusion of the FBP molecules as their binding sites are only attainable from the internal solvent accessible cavity (SAC) of the tetramer. Slices views showing the cavity are presented in Supplementary Fig. S5. Despite the N-terminal extension, *C. apon* LDH assembly adopts an open assembly when unliganded showing that the extensions do not hinder the access to the SAC by the FBP molecules (Fig. 7 B). In the case of *H. sapi* LDH-M, no rearrangements other than the closure of the active loop happens upon substrate analog binding (Fig. 7C).

In conclusion, the *C. apon* LDH N-terminal extensions are not sufficient to shift strongly the allosteric equilibrium toward the R-active state, and consequently hold it in a compact tetrameric form, as it is the case with eukaryotic counterparts.

Its SAC is still accessible and resembles the opening in *B. long* LDH. So, the FBP molecules can diffuse to reach their binding sites and rearrangements will have to happen to force R171 to the IN position.

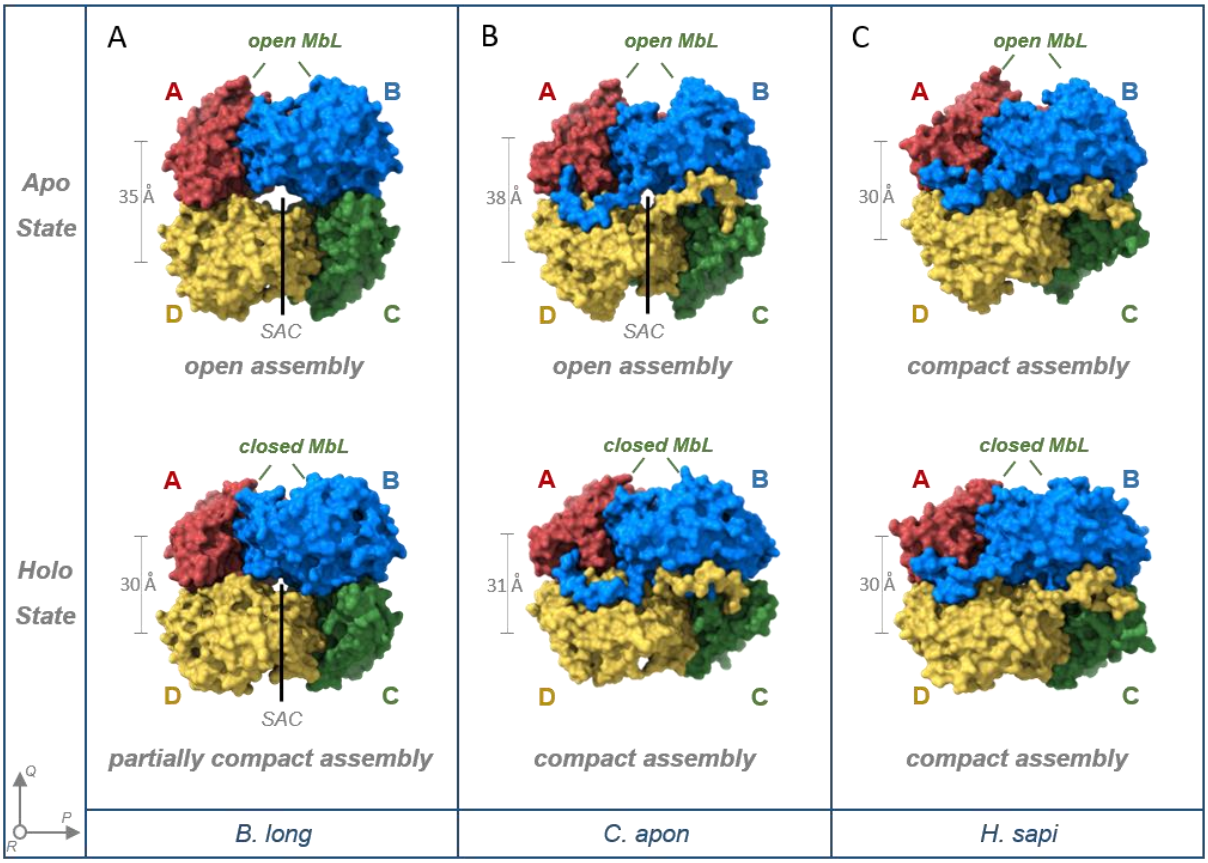

Fig. 7. Surface representation of the tetramers. A) *B. long* LDH. B) *C. apon* LDH. C) *H. sapi* LDH-M with comparison of their Apo and Holo states. To symbolize the compaction along the Q-axis, distances between Cα of A36, a symmetry-related residue at the A//B interface is represented in grey. The tetramer is represented along the *R*-axis. LDH monomers are colored as in Fig. 4.

The deletion of N-terminal extensions affects *C. apon* LDH properties.

In order to evaluate the impact of the N-terminal extensions on the enzyme properties, we designed a mutant in which the N-terminal sequence (MFEKILLSNPSAENPSSLRP) has been deleted (ΔN-ter *C. apon* LDH). We monitored the oligomeric state of ΔN-ter *C. apon* LDH in parallel with the wild type enzyme (Wt *C. apon* LDH) using SEC-MALLS analysis (Fig. 8).

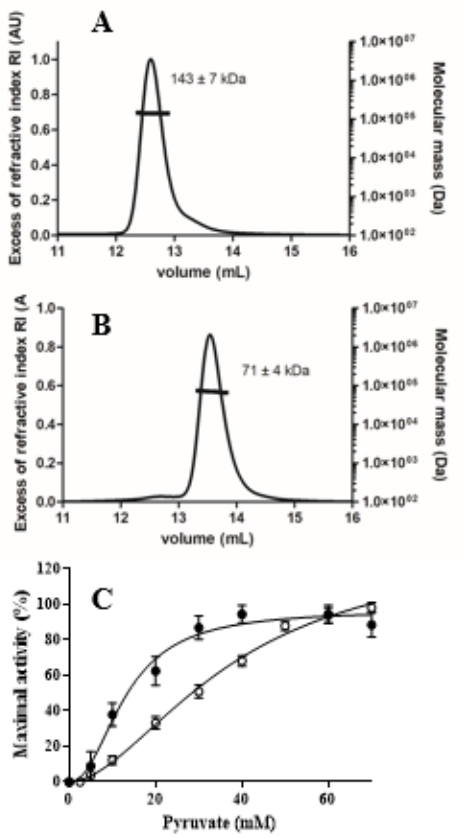

Fig. 8. Effect of N-terminal deletion on enzyme properties. Oligomeric state determination using SEC-MALLS analysis. The chromatogram shows the elution profile monitored by excess refractive index (left ordinate axis) and the molecular weight as dashed line (right ordinate axis) derived from MALLS and refractometry measurements. The estimated average molecular weight is indicated on the graph. (*A*) Wt *C. apon* LDH. (*B*) ΔN-ter *C. apon* LDH. (*C*) Enzymatic activity profiles using pyruvate. Measurements were done in the presence of the indicated concentrations of substrates with NADH as coenzyme. Closed and open circles are for Wt and N-terminal mutant of *C. apon* LDH, respectively.

On the size exclusion column, the ΔN-ter *C. apon* LDH is eluted at a higher volume than *C. apon* wild type LDH, showing it does not behave as a tetramer. The experimental weight-averaged molecular mass of 143 kDa for Wt *C. apon* LDH is close to the theoretical value of 144 kDa for a tetramer (Fig. 8A). In contrast, the value of 71 kDa for the mutant is consistent with a dimeric species instead of a tetramer (Fig. 8B).

We then recorded and compared the pyruvate saturation profile of ΔN-ter *C. apon* LDH with that of Wt *C. apon* LDH (Fig. 8C). The activity profile of the mutant remains sigmoid. However, the K_m value (30mM) for pyruvate is increased for ΔN-ter *C. apon* LDH compared to the wild type enzyme (10mM), demonstrating that the deletion lowers the substrate-binding

affinity of the dimeric species. The k_{cat} value of the ΔN-ter *C. apon* LDH shows the catalytic turnover is lowered compared to the native enzyme (Table S3).

The data demonstrate that the dimeric species is a less efficient enzyme compared to the tetrameric Wt *C. apon* LDH. A similar conclusion was drawn using the ΔN-ter mutant of the *H. sapi* LDH-H (Thabault et al. 2020).

We then tested if the ΔN-ter *C. apon* LDH can be activated by FBP and found no noticeable enhancement of activity when 0.1 or 3 mM FBP was added to the assay (data not shown). These data demonstrate that (i) the N-terminal extensions in *C. apon* LDH contribute to the stability of the tetrameric assembly, which is therefore the prerequisite for the FBP-binding site formation and (ii) that the dimeric species of *C. apon* LDH sustains the homotropic activation. We monitored that deletion of the N-terminal extension lowers the apparent stability by 10°C as assessed by residual activity measurement (Supplementary Table S3). We also designed a *R. chin* ΔN-terminal LDH mutant, but the enzyme did not refold properly preventing its characterization.

Altogether, the complementary structural and biochemical characterizations of new LDHs with N-terminal extensions indicate that their presence is not responsible for the absence of allosteric activation by FBP as it was thought for a long time based on data from *H. sapi* LDH-M only.

Detailing the FBP-binding site.

After demonstrating that there is no link between the absence of allosteric activation by FBP and the presence of the N-terminal extensions, we took a closer look at the AD-like interface which contributes to the formation of the FBP-BS. Structural studies have shown that residues R173, H188, and Y190 of each monomer participate to the binding of FBP (Fig. 9) and can be considered as the signature of the FBP-BS (Iwata and Ohta. 1993; Iwata et al. 1994; Coquelle et al. 2007, Taguchi 2017). These three main residues are present at equivalent position in the *C. apon* LDH sequence. Compared to *C. apon* LDH, *R. chin* and *H. sapi* LDHs show each a single mutation, with the sequences R173, H188Q, and Y190, and R173, H188, and Y190W, respectively. Such variability in the signature sequence may impact the FBP-BS properties of these enzymes. To have a more precise picture, we mapped the presence of the R173, H188, and Y190 onto the LDH phylogeny (Figs. 1 and 2). The corresponding trees show that the majority of bacteria harbor indeed, the FBP-BS amino acids signature (Fig. 1), while in eukaryotes (cluster I and II), the favorable combination is, in most cases, not achieved (Figs. 2 and 9). Even if there are no experimental reports in the literature of LDHs displaying an

(incomplete) amino acids signature unfavorable for FBP binding, we estimate that these kind of LDHs would not be heterotropicaly activated. Consequently, the *P. blak* LDH (table1) displaying both the homo- and heterotropic allosteric activation corresponds therefore, rather to an exception in cluster I (De Arriaga et al. 1982; Soler et al. 1982).

Regarding cluster II, while the FBP-BS signature is present in 88% of the cyanobacterial LDH sequences, it drops-down from 55 to 6% in cluster II eukaryotic lineages (Fig. 9). In fact, the R173 residue is strictly conserved in all cluster II members, while in plants a H188Q replacement and in metazoan a Y190W replacement are observed (Fig. 9). This suggests that these two amino acid positions could play a role in the allosteric capacity changes in eukaryotic LDH irrespective of the N-terminal extension.

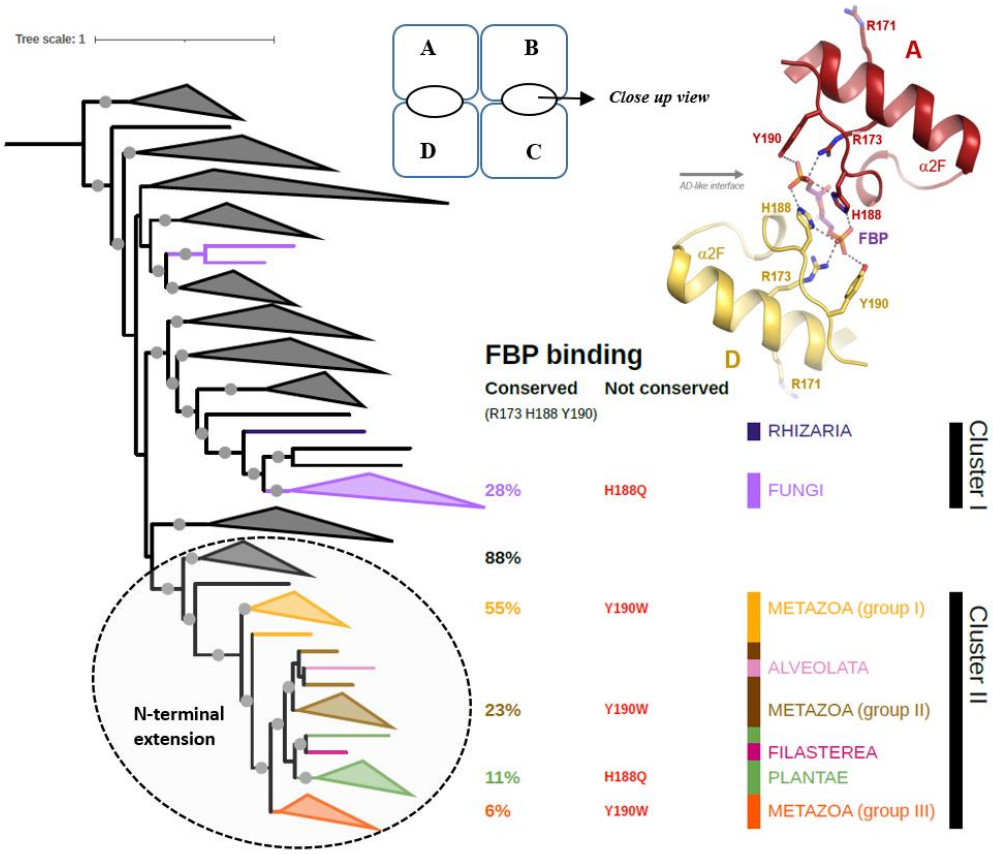

Fig. 9. Conservation of the three critical residues involved in FBP-BS (R173, H188, and Y190) of allosteric bacterial LDH in eukaryotes. For clarity, taxonomic groups have been collapsed. Prokaryotic sequences are in black, while eukaryotic sequences have been colored according to their taxonomy. The conservation of the three residues involved in FBP-BS is reported in % (black). The most frequent alternative amino acids are indicated in red. On the top of the figure, a simplified LDH cartoon indicating the location of FBP-BS and a close up view of the FBP-BS in *C. apon* LDH are shown.

Tuning *C. apon* LDH allosteric properties by single eukaryotic-like mutation

Knowing that *R. chin* LDH that harbor the R173, Q188, Y190 FBP-BS signature has lost the ability to bind FBP but still displays a homotropic behavior, while the activity of the *H. sapi* LDH-M (R173, H188, W190 FBP-BS signature) is not controlled allosterically at neutral pH, we designed two single point mutants, H188Q and Y190W in *C. apon* LDH.

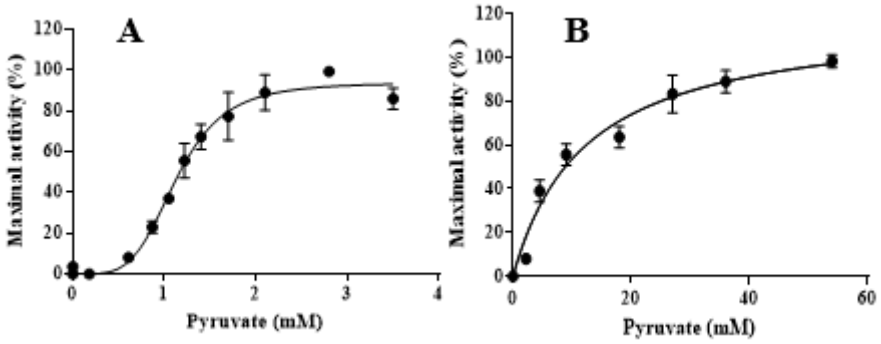

Fig. 10. Catalytic properties of *C. apon* LDH mutants. (*A*) Pyruvate saturation curve for the H188Q mutant, (*B*) Pyruvate saturation curve for the Y190W mutant.

The pyruvate saturation profile of H188Q *C. apon* LDH recorded at pH 7, as for the wild-type enzyme, is sigmoid typical of homotropic activation (Fig. 10A). Yet, this mutant exhibits an unexpected increased affinity for pyruvate with a *K*m value of 1.1 mM compared to the 10 mM value for the wild-type enzyme (Table S3). Such a *K*m value is close to the one determined for the *R. chin* LDH (1.5 mM). We did not record any significant change of activity when the assay was done in the presence of FBP, demonstrating that the H188Q mutation has abolished the FBP-recognition.

The second single mutation Y190W has a strong effect on the *C. apon* LDH enzymatic profile, which becomes hyperbolic (Fig. 10B). However, the pyruvate affinity (Km = 10 mM) stays close to the value obtained with the Wt enzyme. As it was the case with the first mutant, when the assay is done in the presence of FBP, the enzymatic activity of the Y190W *C. apon* LDH mutant was not impacted.

Therefore, introducing each individual mutation of the FBP-BS carried by *R. chin* and *H. sapi* in the sequence of *C. apon* LDH is sufficient to abolish the heterotropic activation by FBP. However, their impact on the T-inactive / R-active state equilibrium is different, with the Y190W mutation inducing a strong shift toward the R-active state.

Structure and electrostatic property changes of the allosteric core.

The non-allosteric properties of vertebrate LDHs have been recently challenged (Iacovino et al. 2022, Pasti et al. 2022). By recording pyruvate saturation profiles, it was found that their hyperbolic shapes turned sigmoidal when measurements were done at low pH values (pH 5), a phenomenon due to the pH-dependent dissociation of the tetramer into dimeric species. Because Y190W *C. apon* LDH can be considered as "mimicking" a vertebrate enzyme, we wondered whether it also displayed pH-dependent allosteric properties. Thus, we compared its pyruvate saturation profiles at pH 5 and 6 with that obtained at pH 7 (Fig. 10). The three profiles were hyperbolic, demonstrating that Y190W *C. apon* LDH activity is not sensitive to pH (Supplementary Figure S6). In addition, we verified that Y190W *C. apon* LDH remains tetrameric in all tested conditions using analytical ultra-centrifugation (Supplementary Figure S6).

Strongly intrigued by the difference of allosteric properties between *C. apon* and *H. sapi* LDH-M induced by the pH conditions, we analysed the occurrence of histidine residues in the close vicinity of the AD-like interfaces that participate to the tetrameric assembly. Indeed, because histidine has a pKa of approximately 6.0, its ionization state may have an influence on the conformational stability. We found that in *H. sapi* LDH-M sequence there are two histidine residues at positions 183 and 218 (Figs. 1 and 2 and Supplementary figures S2, and S4), in the hydrophobic rich region considered as the allosteric core of LDHs (Tagushi 2017, Iorio et al. 2021). They are closely located to the SLE which establishes additional bridging interactions between monomers A and D. In *C. apon* LDH there is no ionisable amino acids in the same region. The structural comparison allows to see that the presence of a SLE in *C. apon* and *H. sapi* LDH-M strongly modify the AlCo structure compared to the conformation observed in *B. long* LDH.

To get insights into their relative effect on allosteric behavior we mapped the presence of these histidine onto the LDH phylogeny (Figs. 1 and 2). Interestingly, they are found almost exclusively in metazoan group III LDHs within cluster II (Fig. 2). More precisely, H183 is found in all metazoan group III sequences, whereas H218 is found in LDH-A. Structurally speaking, due to the symmetry imposed by the tetrameric scaffold, H183 and H218 are located at the P-related interface, so that they make a cluster of eight charges that should be responsible for the pH-dependent dissociation and resulting allosteric transitions as observed in LDH-M

(Iacovino et al. 2022, Pasti et al. 2022). This strongly suggests that the combination of H183 with H218 has a specific role to play in LDH from muscle.

The fate of allosteric regulation in LDHs

Lactate dehydrogenase is an important enzyme catalyzing the reversible conversion of pyruvate into lactate. Deciphering the structure-function relationship of LDH is therefore of great importance to explain their subtle functionality tuning with respect to their various role in cells, in particular in human. Indeed, lactate is a crucial compound for physiological cellular function, metabolism and signal transduction (Adeva-Andany et al. 2014). In particular, alteration of lactate homeostasis participates in human health and disease (reviewed by Li et al. 2022). Consequently, according to Medline, there are more than 43,000 publications devoted to LDHs. In sharp contrast, the number of studies aimed to understand the structure-function evolution of LDH is very low, and in particular, most of those focused on eukaryotic LDH are outdated. The origin of LDH functionality was the result of a malate dehydrogenase gene sequence drift due to a small set of mutations. This phenomenon occurred independently several times (Madern 2002; Boucher et al. 2014; Steindel et al. 2016; Brochier-Armanet et al. 2021). More precisely, phylogenetic analyses have revealed that the clade of stricto sensu LDH evolved from an intermediate group of enzymes, which harbour a mix of functional properties in between the canonical tetrameric MalDHs type 3 and the clade of stricto sensu LDH (Brochier-Armanet and Madern. 2021). The present study shows that canonical LDHs are not uniformly widespread over the three domains of life. They are almost exclusively found in *Bacteria* and *Eucarya*. The most parsimonious scenario suggests that LDH originated from MDH in bacteria and was acquired secondarily via HGT by eukaryotes and a few archaea. The quasi absence of LDHs Archaea is very likely due to strong differences in their carbohydrate metabolism with respect to *Bacteria* and *Eucarya* (Madern 2002; Bräsen et al. 2014). Regarding eukaryotes, two distinct major events led to the LDH in Fungi on the one hand and in other eukaryotes on the other hand.

Previous studies have revealed atypical features of vertebrates LDH (M, H and C forms). Starting from these reports, our work allows depicting the fate of allostery in LDHs. Our survey of the literature indicated that most of the bacterial LDHs display both homotropic and heterotropic activation. Recently, it was shown that the addition of two evolutionary related mutations (strictly found in all LDHs) in a non-allosteric enzyme from the intermediate group with MDH functionality was sufficient to give rise a homotropically activated LDH (Iorio et al 2022). These dynamically-enhancing mutations have changed the conformational equilibrium

of the MDH catalytic site, always found in the R-active state, allowing the resulting new enzyme (i.e. a MDH with LDH capacity) to explore the T-inactive state. In the super family of MDH/LDH, their selection in a non-allosteric ancestral enzyme is considered as the first evolutionary step at the origin of LDHs (Iorio et al 2022). How and when the second set of evolutionary mutations allowing heterotropic activation to emerge from a homotropicaly activated LDHs remains an open question.

The intimate relationship of eukaryotes cluster II LDHs with cyanobacterial LDHs is puzzling as it cannot be linked to the chloroplastic endosymbiosis, i.e. the capture of a cyanobacterial endosymbiont at the origin of plastids in plants and algae. Even if ancient endosymbiotic-independent HGT between eukaryotes and cyanobacteria are considered as rare (Rochette et al. 2014), a recent study has shown that HGT transfer of genes coding for citrullinating enzymes peptidyl arginine deiminases from cyanobacteria to animals introduced new enzymatic regulatory capability through posttranslational modification (Cummings et al. 2022).

The distribution of eukaryotic LDHs into two distinct groups of sequences of different length (with or without N-terminal extensions) raises the question of the benefit of extensions. Contrarily to eukaryote cluster II sequences, fungal sequences belonging to cluster I do not harbor N-terminal extensions. Regarding cluster I, only a single enzyme from fungi (*P. blak*) was characterized and described as activated by FBP (De Arriaga et al. 1982; Soler et al. 1982), and consistently, it harbors the three critical residues in the FBP-BS (R173, H188, and Y190). However, these residues are poorly conserved across cluster I, as 66% of enzymes from cluster I display an incomplete FBP-BS signature. This suggests they have secondarily lost the heterotropic activation capacity. Further investigations will be necessary to describe the evolution of the fungal sequences in more detail.

Our work on *C. apon* LDH revealed that long N-terminal extensions are neither specific of eukaryotes cluster II LDHs nor a structural feature preventing allosteric capacity in LDHs as thought for a long time. In contrast, structural data shows that long N-terminal extension create “staple” like element that is anchored to the AlCo of adjacent monomers. We show that the presence of these extensions impact fold, compactness, and local dynamics of Alco. Accessing new regions of sequence space in enzyme evolution via insertions and deletions is considered as an important mechanism to promote functional and regulatory innovation (Banavali et al. 2005; Vahidi et al. 2018; Emond et al.2020). Owing to that, we suggest that the addition of N-terminal extensions allowed the ancestral eukaryotic LDH to evolve further specific-lineage extinction mechanism of allosteric regulation that would not be achieved without N-terminal

arms. In particular, we observed that the allosteric capacities might be partially or fully switched-off by single mutations that target two positions of the FBP-BS sequence signature at the P-related interface. Our data on *C. apon* illustrates this effect. With respect to allostery, a restricted capacity is observed in plants, as all reports, including our data on *R. chin*, indicate a homotropic activation capacity with an absence of heterotropic activation by FBP (Betsche 1981; Tihannyi et al. 1989; O'Carra and Mulcahy 1995; Sugiyama and Taniguchi, 1997). Moreover, we could indeed recapitulate the plant phenotype with the H188Q *C. apon* LDH mutant, which lose the heterotropic activation by FBP but keep its homotropic activation capacity, demonstrating clearly that a single mutation at position 188 can mimic the partial extinction of the allosteric activation capacity in plants. Note that the absence of regulatory effect by FBP, does not exclude that activity cannot be modulated by different mechanisms such as inhibition by ATP or other metabolites in order to fit metabolic requirements of each plants as observed with lettuce LDH (Betsche, 1981).

Our present work shows that the introduction of the single point mutation, Y190W, in *C. apon* LDH results in completely shifting the enzyme toward the R-active state and thus highlight the role of this residue in vertebrate LDH abolished allosteric capacity. On this basis, LDH from Metazoa group I and III that also display W190 would behave as non-allosteric LDH. Several studies have shown that single amino acid mutations may trigger allosteric activation, i.e. the capacity to explore the T and R states, using non-allosteric (always in the R-state) enzymes as starting point (Kuo et al. 1989; First and Fersht 1993; Zhou et al. 2003, Farsi et al. 2012, Iorio et al. 2022). In contrast, the complete shift of an allosteric enzyme toward an enzyme with Michaelian kinetics i.e. with a strongly reduced capacity to sample the T-state has been rarely documented (Stebbins et al. 1992). In a molecular dynamics study using thermophilic LDHs, it has been shown that the FBP-BS pocket and the allosteric core acts as a tandem of micro switches, controlling the propagation of dynamics and consequently influencing the allosteric capacity (Iorio et al. 2021). The concept of micro switch implies that the allosteric signal propagation may be impacted by changes in small part of an enzyme, frequently hydrophobic rich (Steen et al. 2013; Vogel et al. 2017; White et al. 2018; Mariño Pérez et al. 2021; Fleetwood et al. 2020; Gerrard Wheeler et al. 2021). In these areas, the importance of tryptophan as a key amino acid has been documented in a family of kinases (Chopra et al. 2016). In a work using a transcriptional repressor EthR, the introduction of a W by a single mutation within a small ligand binding pocket was sufficient to shift the enzyme into the R-active state (Carette et al. 2012). We consider therefore that the FBP-BS is a reversible micro switch, depending on the presence or absence of the effector. In eukaryotic LDHs group II, the presence of W190 because

of its bulky side chain, knock down the switching capacity allowing these enzymes to stay constrained into the R-active state.

Recent studies have challenged the concept stating that LDH-A from muscle in vertebrates are non-allosteric enzymes by showing some reminiscent allosteric capacity can be detected, in particular upon low pH-dissociation of the tetrameric state (Katava et al. 2020, Iacovino et al. 2022, Pasti et al. 2022). We noticed that this phenomenon correlates with the apparition of two ionizable histidine (per monomer) in the allosteric core of vertebrates LDHs at position 183 and 218. We suggest that, at low pH, the eight histidine residues mainly located in the close vicinity of the AD-like interfaces are protonated, inducing a local repulsive effect that favors dissociation of the tetramer into A//B dimeric species. A//B-like dimers are less structurally constraint and the opportunity for the enzymes to explore both T-inactive and R-active states reappears. It agrees with the fact that the minimal catalytic unit, which can sustain enzymatic activity, is the A//B dimeric species (Madern et al. 2000). We suggest that the selection of the two histidine residues by muscle LDHs of vertebrate, allowing to be either in a regulated, or a non-regulated state, is a specific adaptive response of muscles subjected to lactic acidosis due to intense exercise.

Our integrative approach demonstrates that linking phylogenetic studies to biochemical and structural information of LDHs have upset their evolutionary history that was previously based on a restricted amount of data.

Author contributions

DM, CBA, and EG conceived the project. DM and CB performed samples preparation, biochemical characterization. DM and AYR performed biophysical characterizations and searched for crystal growth conditions. CBA and DM conducted evolutionary analyses. AYR collected X-rays diffraction data and constructed the resulting structural models. AYR, EG and DM analyzed the structural data. All the authors analyzed the data and wrote the manuscript.

Acknowledgements

The authors acknowledge funding by Agence Nationale de la Recherche (AlloSpace ANR-21-CE44-0034-01). AYR and EG acknowledge Region Auvergne Rhône Alpes for financial support (R&D booster program Crystfrag). AYR and EG also acknowledge Soleil synchrotron and ESRF for beamtime provision and thanks beamline staffs for their help. IBS acknowledges integration into the Interdisciplinary Research Institute of Grenoble (IRIG, CEA).

This work used the platforms of the Grenoble Instruct-ERIC center (ISBG ; UAR 3518 CNRS-CEA-UGA-EMBL) within the Grenoble Partnership for Structural Biology (PSB), supported by FRISBI (ANR-10-INBS-0005-02) and GRAL, financed within the University Grenoble Alpes graduate school CBH-EUR-GS (ANR-17-EURE-0003). We thank Aline Le Roy and/or Christine Ebel, for assistance and/or access to the Analytical Ultracentrifugation (AUC) platform. We thank Olivia Wegrzyniak for her contribution at the starting part of the project.
Part of this work has been performed at the CMBA platform - IRIG-DS-BGE-Gen&Chem-CMBA, CEA-Grenoble, F-38054 Grenoble (a member of GIS-IBISA and ChemBioFrance National Research Infrastructure), which is supported by the LabEX GRAL (Grenoble Alliance for Integrated Structural and Cell Biology), a program of the Chemistry Biology Health Graduate School of Université Grenoble Alpes (ANR-17-EURE-0003).

Conflict of interest

The authors declare that they have no conflicts of interest with the contents of this article.

The data are available in the article and its online supplementary material.

The crystallographic data are deposited at the Protein Data Bank. Accession numbers 8AB2 and 8AB3.

References

Abad-Zapatero C, Griffith JP, Sussman JL, Rossmann MG. 1987. Refined crystal structure of dogfish M4 apo-lactate dehydrogenase. *J Mol Biol.* 198(3):445-467.

Adeva-Andany M, López-Ojén M, Funcasta-Calderón R, Ameneiros-Rodríguez E, Donapetry-García C, Vila-Altesor M, Rodríguez-Seijas J. 2014. Comprehensive review on lactate metabolism in human health. *Mitochondrion*. 17:76-100.

Arai K, Hishida A, Ishiyama M, Kamata T, Uchikoba H, Fushinobu S, Matsuzawa H, Taguchi H. 2002. An absolute requirement of fructose 1, 6-bisphosphate for the *Lactobacillus casei* L-lactate dehydrogenase activity induced by a single amino acid substitution. *Protein Eng.* 15(1):35-41.

Arai K, Ichikawa J, Nonaka S, Miyanaga A, Uchikoba H, Fushinobu S, Taguchi H. 2011. 1 molecular design that stabilizes active state in bacterial allosteric L-lactate dehydrogenases. *J Biochem*. 150(5):579-591.

Arai K, Ishimitsu T, Fushinobu S, Uchikoba H, Matsuzawa H, Taguchi H. 2010. Active and inactive state structures of unliganded Lactobacillus casei allosteric L-lactate dehydrogenase. *Proteins*. 78(3):681-694.

Auerbach G, Ostendorp R, Prade L, Korndörfer I, Dams T, Huber R, Jaenicke R. 1998. Lactate dehydrogenase from the hyperthermophilic bacterium *Thermotoga maritima*: the crystal structure at 2.1 Å resolution reveals strategies for intrinsic protein stabilization. *Structure*. 6(6):769-781.

Banavali NK, Roux B. 2002. The N-terminal end of the catalytic domain of SRC kinase Hck is a conformational switch implicated in long-range allosteric regulation. *Structure.* 13(11):1715-1723.

Betsche T. 1981. L-Lactate dehydrogenase from leaves of higher plants. Kinetics and regulation of the enzyme from lettuce (Lactuca sativa L). *Biochem J*. 195(3):615-622.

Boucher JI, Jacobowitz JR, Beckett BC, Classen S, Theobald DL. 2014. An atomic-resolution view of neofunctionalization in the evolution of apicomplexan lactate dehydrogenases. *Elife*. 3:e02304.

Bräsen C, Esser D, Rauch B, Siebers B. 2014. Carbohydrate metabolism in Archaea: current insights into unusual enzymes and pathways and their regulation. *Microbiol Mol Biol Rev*. 78(1):89-175.

Brochier-Armanet C, Madern D. 2021. Phylogenetics and biochemistry elucidate the evolutionary link between l-malate and l-lactate dehydrogenases and disclose an intermediate group of sequences with mix functional properties. *Biochimie*. 191:140-153.

Burgner JW 2nd, Ray WJ Jr. 1984. On the origin of lactate dehydrogenase induced rate effect. *Biochemistry*. 23: 3636-3648.

Cahn RD, Zwilling E, Kaplan NO, Levine L. 1962. Nature and Development of Lactic Dehydrogenases: The two major types of this enzyme form molecular hybrids, which change in makeup during development. *Science.* 136(3520):962-969.

Callender R, Dyer RB. 2015. The dynamical nature of enzymatic catalysis. *Acc Chem Res*. 48(2):407-413.

Carette X, Blondiaux N, Willery E, Hoos S, Lecat-Guillet N, Lens Z, Wohlkönig A, Wintjens R, Soror SH, Frénois F, Dirié B, Villeret V, England P, Lippens G, Deprez B, Locht C, Willand N, Baulard AR. 2012. Structural activation of the transcriptional repressor EthR from Mycobacterium tuberculosis by single amino acid change mimicking natural and synthetic ligands. *Nucleic Acids Res*. 40(7):3018-3030.

Cendrin F, Chroboczek J, Zaccai G, Eisenberg H, Mevarech M. 1993. Cloning, sequencing, and expression in *Escherichia coli* of the gene coding for malate dehydrogenase of the extremely halophilic archaebacterium Haloarcula marismortui. *Biochemistry* 32:4308–4313.

Chaikuad A, Fairweather V, Conners R, Joseph-Horne T, Turgut-Balik D, Brady RL. 2005. Structure of lactate dehydrogenase from Plasmodium vivax: complexes with NADH and APADH. *Biochemistry*. 44(49):16221-16228.

Chopra N, Wales TE, Joseph RE, Boyken SE, Engen JR, Jernigan RL, Andreotti AH. 2016. Dynamic Allostery Mediated by a Conserved Tryptophan in the Tec Family Kinases. *PLoS Comput Biol.* 12(3):e1004826.

Clarke AR, Atkinson T, Holbrook JJ. 1989. From analysis to synthesis: new ligand binding sites on the lactate dehydrogenase framework. Part I. *Trends Biochem Sci*. 14(3):101-105

Clarke AR, Waldman AD, Hart KW, Holbrook JJ. 1985. The rates of defined changes in protein structure during the catalytic cycle of lactate dehydrogenase. *Biochim Biophys Acta*. 829(3):397-407.

Clarke AR, Wigley DB, Chia WN, Barstow D, Atkinson T, Holbrook JJ. 1986. Site-directed mutagenesis reveals role of mobile arginine residue in lactate dehydrogenase catalysis. *Nature*. 324:699-702.

Clarke AR, Wilks HM, Barstow DA, Atkinson T, Chia WN, Holbrook JJ. 1988. An investigation of the contribution made by the carboxylate group of an active site histidine-aspartate couple to binding and catalysis in lactate dehydrogenase. *Biochemistry*. 27: 1617-1622.

Coquelle N, Fioravanti E, Weik M, Vellieux F, Madern D. 2007. Activity, stability and structural studies of lactate dehydrogenases adapted to extreme thermal environments. *J Mol Biol*. 374(2):547-562.
Criscuolo A, Gribaldo S. 2010. BMGE (Block Mapping and Gathering with Entropy): a new software for selection of phylogenetic informative regions from multiple sequence alignments. *BMC Evol Biol*. 13; 10:210.
Cummings TFM, Gori K, Sanchez-Pulido L, Gavriilidis G, Moi D, Wilson AR, Murchison E, Dessimoz C, Ponting CP, Christophorou MA. 2022. Citrullination Was Introduced into Animals by Horizontal Gene Transfer from Cyanobacteria. *Mol Biol Evol*. 39(2):msab317.

Dacks JB, Field MC, Buick R, Eme L, Gribaldo S, Roger AJ, Brochier-Armanet C, Devos DP. 2016. The changing view of eukaryogenesis - fossils, cells, lineages and how they all come together. *J Cell Sci*. 129(20):3695-3703.
Dawson DM, Goodfriend TL, Kaplan No. 1964. Lactic dehydrogenases: functions of the two types rates of synthesis of the two major forms can be correlated with metabolic differentiation. *Science.* 143 (3609):929-923.

De Arriaga D, Soler J, Cadenas E. 1982. Influence of pH on the allosteric properties of lactate dehydrogenase activity of *Phycomyces blakesleeanus*. *Biochem J*. 203(2):393-400.
Dempster S, Harper S, Moses JE, Dreveny I. 2014. Structural characterization of the apo form and NADH binary complex of human lactate dehydrogenase. *Acta Crystallogr D Biol Crystallogr*. 70(Pt 5):1484-1490.
Deng H, Vu DV, Clinch K, Desamero R, Dyer RB, Callender R. 2011. Conformational heterogeneity within the Michaelis complex of lactate dehydrogenase. *J Phys Chem B.* 115(23):7670-7678.
Deng H, Zheng J, Clarke A, Holbrook JJ, Callender R, Burgner JW 2nd. 1994. Source of catalysis in the lactate dehydrogenase system. Ground-state interactions in the enzyme-substrate complex. *Biochemistry*. 33(8):2297-2305.
Egawa T, Deng H, Chang E, Callender R. 2019. Effect of Protein Isotope Labeling on the Catalytic Mechanism of Lactate Dehydrogenase. *J Phys Chem B*. 123(46):9801-9808.
Emond S, Petek M, Kay EJ, Heames B, Devenish SRA, Tokuriki N, Hollfelder F. 2020. Accessing unexplored regions of sequence space in directed enzyme evolution via insertion/deletion mutagenesis. *Nat Commun*. 11(1):3469.
Emsley P, Lohkamp B, Scott WG, Cowtan K. 2010. Features and development of Coot. *Acta Crystallogr D Biol Crystallogr*. 66(Pt 4):486-501.

Engilberge S, Riobé F, Di Pietro S, Lassalle L, Coquelle N, Arnaud CA, Pitrat D, Mulatier JC, Madern D, Breyton C, Maury O, Girard E. 2017. Crystallophore: a versatile lanthanide complex for protein crystallography combining nucleating effects, phasing properties, and luminescence. *Chem Sci.* 8(9):5909-5917.

Eszes CM, Sessions RB, Clarke AR, Moreton KM, Holbrook JJ. 1996. Removal of substrate inhibition in a lactate dehydrogenase from human muscle by a single residue change. *FEBS Lett*. 399(3):193-197.

Eventoff W, Rossmann MG, Taylor SS, Torff HJ, Meyer H, Keil W, Kiltz HH.1977. Structural adaptations of lactate dehydrogenase isozymes. *Proc Natl Acad Sci U S A.* 74(7):2677-2681.

Everse, J. and Kaplan, NO. 1973. Lactate dehydrogenases: structure and function. *Adv. Enzym. Mol. Biol.* 37, 61–133.

Farsi Z, Pein H, Pazhang M, Zareian S, Ranaei-Siadat SO, Khajeh K. 2012. Conferral of allostery to Thermus sp. GH5 methylglyoxal synthase by a single mutation. *J Biochem*. 152(6):531-538.

Feldman-Salit A, Hering S, Messiha HL, Veith N, Cojocaru V, Sieg A, Westerhoff HV, Kreikemeyer B, Wade RC, Fiedler T. 2013. Regulation of the activity of lactate dehydrogenases from four lactic acid bacteria. *J Biol Chem.* 288(29):21295-21306.

Fersht, A. 1985. Enzyme structure and mechanism. 2nd, ed, New York: edition Freeman and Co.

First EA, Fersht AR. 1993. Mutation of lysine 233 to alanine introduces positive cooperativity into tyrosyl-tRNA synthetase. *Biochemistry*. 32(49):13651-13657.

Fleetwood O, Matricon P, Carlsson J, Delemotte L. 2020. Energy Landscapes Reveal Agonist Control of G Protein-Coupled Receptor Activation via Microswitches. Biochemistry. 59(7):880-891.

Frauenfelder H, McMahon BH, Austin RH, Chu K, Groves JT. 2001. The role of structure, energy landscape, dynamics, and allostery in the enzymatic function of myoglobin. *Proc Natl Acad Sci U S A*. 98(5):2370-2374.

Friberg A, Rehwinkel H, Nguyen D, Pütter V, Quanz M, Weiske J, Eberspächer U, Heisler I, Langer G. 2020. Structural Evidence for Isoform-Selective Allosteric Inhibition of Lactate Dehydrogenase A. *ACS Omega*. 5(22):13034-13041.

Fushinobu S, Kamata K, Iwata S, Sakai H, Ohta T, Matsuzawa H. 1996. Allosteric activation of L-lactate dehydrogenase analyzed by hybrid enzymes with effector-sensitive and -insensitive subunits. *J Biol Chem*. 271(41):25611-25616.

Garvie EI. 1980. Bacterial lactate dehydrogenases. *Microbiol Rev*. 44(1):106-39.

Gerrard Wheeler MC, Arias CL, E Mello JDFR, Cirauqui Diaz N, Rodrigues CR, Drincovich MF, de Souza AMT, Alvarez CE. 2021. Structural insights into the allosteric site of Arabidopsis NADP-malic enzyme 2: role of the second sphere residues in the regulatory signal transmission. *Plant Mol Biol.* 107(1-2):37-48.

Goto T, Sugawara K, Nakamura S, Kidokoro SI, Wakui H, Nunomura W. 2016. Enzymatic and thermodynamic profiles of a heterotetramer lactate dehydrogenase isozyme in swine. *Biochem Biophys Res Commun*. 479(4):860-867.

Guo J, Zhou HX. 2016. Protein Allostery and Conformational Dynamics. *Chem Rev*. 116(11):6503-6515.

Holbrook JJ, Liljas A, Steindel SJ, Rossmann MG. 1975. Lactate Dehydrogenase. In: Boyer PD, editor. The Enzymes. New York: Academic Press. p. 191–292.

Holland LZ, McFall-Ngai M, Somero GN. 1997. Evolution of lactate dehydrogenase-A homologs of barracuda fishes (genus Sphyraena) from different thermal environments: differences in kinetic properties and thermal stability are due to amino acid substitutions outside the active site. *Biochemistry*. 36(11):3207-15.

Hondred D, Hanson AD. 1990. Hypoxically inducible barley lactate dehydrogenase: cDNA cloning and molecular analysis. *Proc Natl Acad Sci U S A*. 87(18):7300-7304.

Iacovino LG, Rossi M, Di Stefano G, Rossi V, Binda C, Brigotti M, Tomaselli F, Pasti AP, Dal Piaz F, Cerini S, Hochkoeppler A. 2022. Allosteric transitions of rabbit skeletal muscle lactate dehydrogenase induced by pH-dependent dissociation of the tetrameric enzyme. *Biochimie*. 199:23-35.

Ikehara Y, Arai K, Furukawa N, Ohno T, Miyake T, Fushinobu S, Nakajima M, Miyanaga A, Taguchi H. 2014. The core of allosteric motion in Thermus caldophilus L-lactate dehydrogenase. *J Biol Chem*. 289(45):31550-31564.

Iorio A, Roche J, Engilberge S, Coquelle N, Girard E, Sterpone F, Madern D. 2021. Biochemical, structural and dynamical studies reveal strong differences in the thermal-dependent allosteric behavior of two extremophilic lactate dehydrogenases. *J Struct Biol.* 213(3):107769.

Iwasaki Y, Kita A, Yoshida K, Tajima T, Yano S, Shou T, Saito M, Kato J, Murakami K, Nakashimada Y. 2017. Homolactic Acid Fermentation by the Genetically Engineered Thermophilic Homo acetogen Moorella thermoacetica ATCC 39073. Appl Environ Microbiol. 83(8):e00247-17.

Iwata S, Kamata K, Yoshida S, Minowa T, Ohta T. 1994. T and R states in the crystals of bacterial L-lactate dehydrogenase reveal the mechanism for allosteric control. *Nat Struct Biol*. 1(3):176-185.

Iwata S, Ohta T. 1993. Molecular basis of allosteric activation of bacterial L-lactate dehydrogenase. *J Mol Biol*. 230(1):21-27.

Iwata S, Yoshida S, Ohta T. 1994. A regular 1:1 complex of two allosteric states in the single crystal of L-lactate dehydrogenase from Bifidobacterium longum. *J Mol Biol*. 236(3):958-959.

Iyer A, Reis RAG, Gannavaram S, Momin M, Spring-Connell AM, Orozco-Gonzalez Y, Agniswamy J, Hamelberg D, Weber IT, Gozem S, Wang S, Germann MW, Gadda G. A. 2021. Single-Point Mutation in d-Arginine Dehydrogenase Unlocks a Transient Conformational State Resulting in Altered Cofactor Reactivity. *Biochemistry*. 60(9):711-724.

Kabsch W. 2010. XDS. *Acta Crystallogr D Biol Crystallogr*. 66(Pt 2):125-32.

Kalyaanamoorthy S, Minh BQ, Wong TKF, von Haeseler A, Jermiin LS. 2017. ModelFinder: fast model selection for accurate phylogenetic estimates. *Nat Methods*. 14(6):587-589.

Karvountzi E, Kilias G, Alahiotis SN. 1995. Drosophila lactate dehydrogenase. Functional and evolutionary aspects. *Hereditas*. 123(1):61-67.

Katava M, Maccarini M, Villain G, Paciaroni A, Sztucki M, Ivanova O, Madern D, Sterpone F. 2017. Thermal activation of 'allosteric-like' large-scale motions in a eukaryotic Lactate Dehydrogenase. *Sci Rep*. 7:41092.

Katava M, Marchi M, Madern D, Sztucki M, Maccarini M, Sterpone F. 2020. Temperature Unmasks Allosteric Propensity in a Thermophilic Malate Dehydrogenase via Dewetting and Collapse. *J Phys Chem B*. 124(6):1001-1008.

Katoh K, Standley DM. 2013. MAFFT multiple sequence alignment software version 7: improvements in performance and usability. *Mol Biol Evol*. 30(4):772-780.

Kolappan S, Shen DL, Mosi R, Sun J, McEachern EJ, Vocadlo DJ, Craig L. 2015. Structures of lactate dehydrogenase A (LDHA) in apo, ternary and inhibitor-bound forms. *Acta Crystallogr D Biol Crystallogr*. 71(2):185-195.

Kuo LC, Zambidis I, Caron C. 1989. Triggering of allostery in an enzyme by a point mutation: ornithine transcarbamoylase. *Science*. 245(4917):522-524.
Le Roy A, Wang K, Schaack B, Schuck P, Breyton C, Ebel C. 2015. AUC and Small-Angle Scattering for Membrane Proteins. *Methods Enzymol*. 562:257-286.
Letunic I, Bork P. 2021. Interactive Tree Of Life (iTOL) v5: an online tool for phylogenetic tree display and annotation. *Nucleic Acids Res.* 49(W1):W293-W296.
LeVan KM, Goldberg E. 1991. Properties of human testis-specific lactate dehydrogenase expressed from Escherichia coli. *Biochem J.* 273 (Pt 3)(Pt 3):587-592.
Li X, Yang Y, Zhang B, Lin X, Fu X, An Y, Zou Y, Wang JX, Wang Z, Yu T. 2022. Lactate metabolism in human health and disease. *Signal Transduct Target Ther*. 7(1):305.

Madern D, Cai XM, Abrahamsen MS, Zhu G. 2004. Evolution of *Cryptosporidium parvum* lactate dehydrogenase from malate dehydrogenase by a very recent event of gene duplication. *Mol Biol Evol* 21: 489-497.
Madern D, Ebel C, Mevarech M, Richard SB, Pfister C, Zaccai G. 2000. Insights into the molecular relationships between malate and lactate dehydrogenases: structural and biochemical properties of monomeric and dimeric intermediates of a mutant of tetrameric L-[LDH-like] malate dehydrogenase from the halophilic archaeon Haloarcula marismortui. Biochemistry. 39(5):1001-1010.

Madern D. 2002. Molecular Evolution within the L-Malate and L-Lactate Dehydrogenase Super-Family. *J Mol Evol* 54: 825-840.
Mariño Pérez L, Ielasi FS, Bessa LM, Maurin D, Kragelj J, Blackledge M, Salvi N, Bouvignies G, Palencia A, Jensen MR. 2022. Visualizing protein-breathing motions associated with aromatic ring flipping. *Nature*. 602(7898):695-700.
Matoba Y, Miyasako M, Matsuo K, Oda K, Noda M, Higashikawa F, Kumagai T, Sugiyama M. 2014. An alternative allosteric regulation mechanism of an acidophilic l-lactate dehydrogenase from *Enterococcus mundtii* 15-1A. *FEBS Open Bio*. 4:834-847.
McClendon S, Zhadin N, Callender R. 2005. The approach to the Michaelis complex in lactate dehydrogenase: the substrate binding pathway. *Biophys J*. 89(3):2024-2032.
Monod J, Wyman J, Changeux JP. 1965. On the nature of allosteric transitions, a plausible model. *J Mol Biol*. 12: 88-118.
Morin A, Eisenbraun B, Key J, Sanschagrin PC, Timony MA, Ottaviano M, Sliz P. 2013. Collaboration gets the most out of software. Elife. 2:e01456.

Motlagh HN, Wrabl JO, Li J, Hilser VJ. 2014. The ensemble nature of allostery. *Nature*. 508(7496):331-339.
Nguyen LT, Schmidt HA, von Haeseler A, Minh BQ. 2015. IQ-TREE: a fast and effective stochastic algorithm for estimating maximum-likelihood phylogenies. *Mol Biol Evol*. 32(1):268-274.
Nowicki MW, Blackburn EA, McNae IW, Wear MA. 2015. A Streamlined, Automated Protocol for the Production of Milligram Quantities of Untagged Recombinant Rat Lactate Dehydrogenase A Using ÄKTAxpressTM. PLoS One. 10(12):e0146164.

Nussinov R, Ma B, Tsai CJ. 2014. Multiple conformational selection and induced fit events take place in allosteric propagation. *Biophys Chem*. 186:22-30.
O'Carra P, Mulcahy P. 1996. Lactate dehydrogenase in Plants: distribution and function. *Phytochemistry*. 42(3):581-587.
Ozkan M, Yilmaz EI, Lynd LR, Ozcengiz G. 2004. Cloning and expression of the Clostridium thermocellum L-lactate dehydrogenase gene in Escherichia coli and enzyme characterization. Can J Microbiol. 50(10):845-851.
Pasti AP, Rossi V, Di Stefano G, Brigotti M, Hochkoeppler A. 2022. Human lactate dehydrogenase A undergoes allosteric transitions under pH conditions inducing the dissociation of the tetrameric enzyme. *Biosci Rep*. 42(1):BSR20212654.
Pesce A, Fondy TP, Stolzenbach F, Castillo F, Kaplan NO. 1967. The comparative enzymology of lactic dehydrogenases. 3. Properties of the H4 and M4 enzymes from a number of vertebrates. *J Biol Chem*. 242(9):2151-2167.
Pineda JR, Callender R, Schwartz SD. 2007. Ligand binding and protein dynamics in lactate dehydrogenase. *Biophys J*. 93(5):1474-1483.
Piontek K, Chakrabarti P, Schär HP, Rossmann MG, Zuber H. 1990. Structure determination and refinement of *Bacillus stearothermophilus* lactate dehydrogenase. *Proteins*. 7(1):74-92.
Read JA, Winter VJ, Eszes CM, Sessions RB, Brady RL. 2001. Structural basis for altered activity of M- and H-isozyme forms of human lactate dehydrogenase. *Proteins*. 43(2):175-185.
Rochette NC, Brochier-Armanet C, Gouy M. 2014. Phylogenomic test of the hypotheses for the evolutionary origin of eukaryotes. *Mol Biol Evol*. 31(4):832-845.
Rolstad AK, Howland E, Sirevag R. 1988. Malate dehydrogenase from the thermophilic green bacterium Chloroflexus aurantiacus: purification, molecular weight, amino acid composition, and partial amino acid sequence, *J. Bact*. 170: 2947-2953.

Rossmann MG, Adams MJ, Buehner M, Ford GC, Hackert ML, Liljas A, Rao ST, Banaszak LJ, Hill E, Tsernoglou D, Webb L. 1973. Letter: Molecular symmetry axes and subunit interfaces in certain dehydrogenases. *J Mol Biol*. 76(4):533-537.

Sakai I, Sharief FS, Li SS. 1987. Molecular cloning and nucleotide sequence of the cDNA for sperm-specific lactate dehydrogenase-C from mouse. *Biochem J*. 242(2):619-622.

Schroeder G, Matsuzawa H, Ohta T. 1988. Involvement of the conserved histidine-188 residue in the L-lactate dehydrogenase from *Thermus caldophilus* GK24 in allosteric regulation by fructose 1,6-bisphosphate. *Biochem Biophys Res Commun*.152 (3):1236-1241.

Soler J, De Arriaga D, Busto F, Cadenas E. 1982. Lactate dehydrogenase in *Phycomyces blakesleeanus*. *Biochem J*. 203(2):383-391.

Stebbins JW, Kantrowitz ER. 1992. Conversion of the non-cooperative *Bacillus subtilis* aspartate transcarbamoylase into a cooperative enzyme by a single amino acid substitution. Biochemistry. 31(8):2328-2332.

Steen A, Thiele S, Guo D, Hansen LS, Frimurer TM, Rosenkilde MM. 2013. Biased and constitutive signaling in the CC-chemokine receptor CCR5 by manipulating the interface between transmembrane helices 6 and 7. *J Biol Chem*. 288:12511–12521.

Steindel PA, Chen EH, Wirth JD, Theobald DL. 2016. Gradual neofunctionalization in the convergent evolution of trichomonad lactate and malate dehydrogenases. *Protein Sci*. 25(7):1319-1331.

Stock DW, Quattro JM, Whitt GS, Powers DA. 1997. Lactate dehydrogenase (LDH) gene duplication during chordate evolution: the cDNA sequence of the LDH of the tunicate Styela plicata. *Mol Biol Evol*. 14(12):1273-1284.

Sugiyama N, Taniguchi N. 1997. Evaluation of the role of lactate dehydrogenase in oxalate synthesis. *Phytochemistry*. 44(4):571-574.

Swiderek K, Panczakiewicz A, Bujacz A, Bujacz G, Paneth P. 2009. Modeling of isotope effects on binding oxamate to lactic dehydrogenase. *J Phys Chem B*. 113(38):12782-12789.

Taguchi H, Ohta T. 1992. Unusual amino acid substitution in the anion-binding site of Lactobacillus plantarum non-allosteric L-lactate dehydrogenase. *Eur J Biochem*. 209(3):993-998.

Taguchi H. 2017. The Simple and Unique Allosteric Machinery of *Thermus caldophilus* Lactate Dehydrogenase: Structure-Function Relationship in Bacterial Allosteric LDHs. *Adv Exp Med Biol*. 925:117-145.

Talon R, Coquelle N, Madern D, Girard E. 2014. An experimental point of view on hydration/solvation in halophilic proteins. *Front Microbiol*. 5:66.
Thabault L, Brisson L, Brustenga C, Martinez Gache SA, Prévost JRC, Kozlova A, Spillier Q, Liberelle M, Benyahia Z, Messens J, Copetti T, Sonveaux P, Frédérick R. 2020. Interrogating the Lactate Dehydrogenase Tetramerization Site Using (Stapled) Peptides. *J Med Chem*. 63(9):4628-4643
Tihanyi K, Fontanell A, Talbot B, Thirion JP. 1989. Soybean L-(+)-lactate dehydrogenases: purification, characterization, and resolution of subunit structure. *Arch Biochem Biophys.* 274(2):626-632.
Tsoi SC, Li SS. 1994.The nucleotide and deduced amino-acid sequences of a cDNA encoding lactate dehydrogenase from Caenorhabditis elegans: the evolutionary relationships of lactate dehydrogenases from mammals, birds, amphibian, fish, nematode, plants, bacteria, mycoplasma, and plasmodium. *Biochem Biophys Res Commun*. 205(1):558-564.
Tsuji S, Qureshi MA, Hou EW, Fitch WM, Li SS. 1994. Evolutionary relationships of lactate dehydrogenases (LDHs) from mammals, birds, an amphibian, fish, barley, and bacteria: LDH cDNA sequences from Xenopus, pig, and rat. *Proc Natl Acad Sci U S A*. 91(20):9392-9396.
Uchikoba H, Fushinobu S, Wakagi T, Konno M, Taguchi H, Matsuzawa H. 2002. Crystal structure of non-allosteric L-lactate dehydrogenase from *Lactobacillus pentosus* at 2.3 Å resolution: specific interactions at subunit interfaces. *Proteins*. 46(2):206-214.
Vahidi S, Ripstein ZA, Bonomi M, Yuwen T, Mabanglo MF, Juravsky JB, Rizzolo K, Velyvis A, Houry WA, Vendruscolo M, Rubinstein JL, Kay LE. 2018. Reversible inhibition of the ClpP protease via an N-terminal conformational switch. *Proc Natl Acad Sci U S A.* 115(28):E6447-E6456.
VanBeek J, Callender R, Gunner MR. 1997. The contribution of electrostatic and van der Waals interactions to the stereospecificity of the reaction catalyzed by lactate dehydrogenase. *Biophys J*. 72(2):619-626.
Vesell ES. 1965. Lactate dehydrogenase Isozymes: substrate inhibition in various human tissues. *Science*. 150(3703):1590-1593.
Vogel M, Bukau B, Mayer MP. 2006. Allosteric regulation of Hsp70 chaperones by a proline switch. *Mol Cell*. 21(3):359-367.
White KL, Eddy MT, Gao ZG, Han GW, Lian T, Deary A, Patel N, Jacobson KA, Katritch V, Stevens RC. 2018. Structural Connection between Activation Microswitch and Allosteric Sodium Site in GPCR Signaling. *Structure*. 26(2):259-269.e5.

Wigley DB, Gamblin SJ, Turkenburg JP, Dodson EJ, Piontek K, Muirhead H, Holbrook JJ. 1992. Structure of a ternary complex of an allosteric lactate dehydrogenase from *Bacillus stearothermophilus* at 2.5 Å resolution. *J Mol Biol*. 223(1):317-335.

Wilks HM, Hart KW, Feeney R, Dunn CR, Muirhead H, Chia WN, Barstow DA, Atkinson T, Clarke AR, Holbrook JJ. 1988. A specific, highly active malate dehydrogenase by redesign of a lactate dehydrogenase framework. *Science*. 242:1541–1544.

Winn MD, Ballard CC, Cowtan KD, Dodson EJ, Emsley P, Evans PR, Keegan RM, Krissinel EB, Leslie AG, McCoy A, McNicholas SJ, Murshudov GN, Pannu NS, Potterton EA, Powell HR, Read RJ, Vagin A, Wilson KS. 2011. Overview of the CCP4 suite and current developments. *Acta Crystallogr D Biol Crystallogr*. 67(Pt 4):235-42.

Wuntch T, Chen RF, Vesell ES. 1970. Lactate dehydrogenase isozymes: further kinetic studies at high enzyme concentration. Science. 169(3944):480-481.

Yeswanth S, Nanda Kumar Y, Venkateswara Prasad U, Swarupa V, Koteswara rao V, Venkata Gurunadha Krishna Sarma P. 2013. Cloning and characterization of l-lactate dehydrogenase gene of Staphylococcus aureus. *Anaerobe*. 24:43-48.

Zheng Y, Guo S, Guo Z, Wang X. Effects of N-terminal deletion mutation on rabbit muscle lactate dehydrogenase. Biochemistry (Mosc). 2004 Apr;69(4):401-6.

Zhou Y, Zhou H, Karplus M. 2003. Cooperativity in Scapharca dimeric hemoglobin: simulation of binding intermediates and elucidation of the role of interfacial water. *J Mol Biol*. 326(2):593-606.